SYNTHESIS OF COATED NANOPARTICLES FOR THE OXIDATIVE DENITROGENATION OF FUELS

Ana Júlia Briganti Bezerra

Dissertation report presented to

Escola Superior de Tecnologia e Gestão

Instituto Politécnico de Bragança

to obtain a Master's Degree in

Chemical Engineering

within the scope of the double degree program with

Universidade Tecnológica Federal do Paraná

Supervisors:

Prof. Dr. Helder Teixeira Gomes

Prof. Dra. Renata Mello Giona

Bragança

2024

ACKNOWLEDGEMENTS

Firstly, I would like to thank God for guiding and protecting me along this entire journey.

There are no words that can fully express the depth of my gratitude to my parents, Juliana and Anderson, who crossed limits so I could realize dreams they didn't even know were possible. They gave me support, education, love and wings to fly, and always remind me that no matter how far I fly, I have a home to come back to. I am who I am because of you and for that I am infinitely grateful.

To my love, Gabriel, thank you for believing in me even when I don't, for holding my hand and never letting me give up, your support over all these years has kept me strong and motivated. You and our Alfred are my safe haven, and I can't wait to build and make even more dreams come true with you by my side.

Gratitude to my supervisors, Professor Dr. Helder Teixeira Gomes, from the Instituto Politécnico de Bragança (IPB), and Professor Dra. Renata Mello Giona, from the Universidade Tecnológica Federal do Paraná (UTFPR), for their support, trust and guidance in carrying out this work.

To my colleagues in the laboratory, especially Msc. Fernanda Roman, for all her dedication, patience and teachings in developing this project, thank you for guiding me through every stage of the process.

My sincerest thanks to all my family - my aunts, uncles and cousins - for their support and love. To my grandparents, Angela, Vanilda and Expedito, for their love and tireless prayers, and to my grandfather Mauro, who looks after me from heaven and I love and miss so much.

To my friends, who have supported me not only during my master's journey, but during all the things I've already decided to do academically. A special thanks to my friend-sister Bianca, who, despite being far away and not understanding engineering, was always there to listen and support me and listen to 5-minute audios.

I would also like to extend my sincere gratitude to the Universidade Tecnológica Federal do Paraná, especially my professors at the campus in Campo Mourão, as well as the the Instituto Politécnico de Bragança. The opportunity to be here and to obtain a double degree has been a dream since I was 15, and the enriching academic experiences at both institutions have been fundamental to my growth. Learning in another country was a life-changing experience and I am deeply grateful for it.

Finally, to everyone who has been mentioned here and to everyone who has been part of this journey in any way - thank you from the bottom of my heart.

To my “vô Mauro”, I hope that on the radios in heaven you can tell everyone that your n° 1 is a master in chemical engineering.

ABSTRACT

The presence of nitrogen compounds in fossil fuels leads to the formation of NOx during combustion, harmful pollutants that represent a significant challenge for the environment and health, making its removal very important. Hydrotreatment, currently the most common strategy for denitrogenation, requires severe operating conditions, which motivates the search for more sustainable alternatives. This study investigates oxidative denitrogenation (ODN) as a promising strategy, analyzing the oxidation of quinoline, a nitrogen-containing compound common in fossil fuels, using catalysts based cobalt ferrite and its variants coated with silica ($CoFe_2O_4@SiO_2$) and carbon ($CoFe_2O_4@C$), applied in a biphasic system containing isooctane as the organic phase and hydrogen peroxide as the oxidant. Cobalt ferrite was synthesized using the sol-gel method, followed by silica and carbon coatings. Characterization techniques such as XRD, FTIR and contact angle measurements confirmed the successful synthesis of core-shell structures, with crystallite sizes in the 19-20 nm range. The coatings significantly modified the surface properties, reducing the hydrophobicity of the ferrite, with the contact angle reduced from 130° to 40° with silica. Quinoline adsorption tests revealed a low adsorption capacity of the materials, in line with the low surface area and low pore volume determined by N_2 adsorption isotherms at 77 K (S_{BET} = 9-10 m^2/g). In the oxidation reactions, $CoFe_2O_4@SiO_2$ showed the best catalytic performance removing 74% of quinoline in 8 hours, likely due to its hydrophilic surface, favorable to the generation of reactive oxygen species through the decomposition of H_2O_2 and consequent greater quinoline removal. GC-MS identified intermediate degradation products, including species suggesting the opening of pyridine rings, while TOC analysis confirmed significant quinoline mineralization. The study highlights the potential of oxidative denitrogenation systems, combined with coated catalysts, to effectively remove nitrogen impurities from liquid fuels, offering a promising alternative to conventional hydrotreatment.

Keywords: Oxidative denitrogenation, cobalt ferrite, biphasic system, coated catalysts.

RESUMO

A presença de compostos azotados nos combustíveis fósseis leva à formação de NOx durante a combustão, poluentes nocivos que representam um desafio significativo para o ambiente e para a saúde, tornando a sua remoção muito importante. O hidrotratamento, atualmente a estratégia mais comum para a desnitrogenação, requer condições de operação severas, o que motiva a procura de alternativas mais sustentáveis. Este estudo investiga a desnitrogenação oxidativa (ODN) como uma estratégia promissora, analisando a oxidação da quinolina, um composto contendo azoto comum em combustíveis fósseis, utilizando catalisadores baseados em ferrite de cobalto e suas variantes revestidas com sílica ($CoFe_2O_4@SiO_2$) e carbono ($CoFe_2O_4@C$) , aplicados num sistema bifásico contendo isooctano como fase orgânica e peróxido de hidrogénio como oxidante. A ferrite de cobalto foi sintetizada pelo método sol-gel, seguida de revestimentos de sílica e carbono. As técnicas de caraterização, tais como XRD, FTIR e medições do ângulo de contacto, confirmaram a síntese bem sucedida de estruturas core-shell, com tamanhos de cristalitos na gama de 19-20 nm. Os revestimentos modificaram significativamente as propriedades da superfície, reduzindo a hidrofobicidade da ferrite, com o ângulo de contacto reduzido de 130° para 40° com sílica. Os testes de adsorção de quinolina revelaram uma baixa capacidade de adsorção dos materiais, em conformidade com a baixa área superficial e o baixo volume de poros determinados pelas isotérmicas de adsorção de N_2 a 77 K (S_{BET} = 9-10 m^2/g). Nas reacções de oxidação, o $CoFe_2O_4@SiO_2$ apresentou o melhor desempenho catalítico, removendo 74% da quinolina em 8 horas, possivelmente relacionado à sua superfície hidrofílica, favorável à geração de espécies reactivas de oxigénio através da decomposição do H_2O_2 e consequente maior remoção da quinolina. O GC-MS identificou produtos de degradação intermédios, incluindo espécies que sugerem a abertura de anéis de piridina, enquanto a análise do TOC confirmou uma mineralização significativa da quinolina. O estudo mostra o potencial dos sistemas de desnitrogenação oxidativa, combinados com catalisadores revestidos, para remover eficazmente as impurezas azotadas dos combustíveis líquidos, oferecendo uma alternativa promissora ao hidrotratamento convencional.

Palavras-chave: Desnitrogenação oxidativa, ferrite de cobalto, sistema bifásico, catalisadores revestidos.

LIST OF CONTENTS

LIST OF FIGURES

LIST OF TABLES

LIST OF ACRONYMS

ADN	Adsorptive denitrogenation
BDN	Biodenitrogenation
BET	Brunauer-Emmett-Teller method
ECODN	Extractive catalytic oxidative denitrogenation
EDN	Extractive denitrogenation
FTIR	Fourier transform infrared spectroscopy
GC-FID	Gas chromatography-flame ionization detection
GC-MS	Gas chromatography-mass spectrometry
HDN	Hydrodenitrogenation
HDS	Hydrodesulfurization
HPLC	High-performance liquid chromatography
ILs	Ionic liquid extraction
IUPAC	International Union of Pure and Applied Chemistry
N.C.	Non-catalytic
NOx	Nitrogen oxides
ODN	Oxidative denitrogenation
QN	Quinoline
S_{BET}	Surface area by BET
SEM	Scanning electron microscopy
SOx	Sulfur oxides
TEM	Transmission electron microscopy
TEOS	Tetraethyl orthosilicate
TGA	Thermogravimetric analysis
TOC	Total organic carbon
UV-VIS	Ultraviolet-visible spectroscopy
XRD	X-ray diffraction

INTRODUCTION

1. INTRODUCTION

The presence of impurities in petroleum-based fuels, such as nitrogen, represents a significant challenge due to the associated environmental and health impacts. The current process for removing these unwanted species from liquid fuels, known as hydrotreating, requires severe operating conditions for the complete removal of nitrogen. It is therefore imperative to explore viable alternatives to this process. In this context, *oxidative denitrogenation* (ODN) emerges as a suitable solution, especially as it employs milder conditions (25-120 °C, 1-2 bar) and the oxidative reactivity of nitrogen compounds.

ODN is commonly carried out in a two-step process, but it can be optimized using a two-phase system, consisting of an organic phase (fuel) and an aqueous phase containing the oxidant, such as hydrogen peroxide. This configuration requires the use of suitable catalysts that increase contact between the oxidizer and the pollutant. Ideally, these catalysts should be composed of active sites that facilitate the degradation of hydrogen peroxide into highly reactive hydroxyl radicals.

An example of an effective catalyst is cobalt ferrite, known for its ability to catalyze the decomposition of hydrogen peroxide. However, to ensure a more efficient interaction with the hydrophobic pollutant and to avoid the leaching of metallic species, it is possible to coat the cobalt ferrite with a suitable shell, such as carbon or silica.

Therefore, the use of ODN systems, combined with appropriate catalysts and process optimization techniques, represents a promising approach for the effective removal of nitrogen impurities from liquid fuels, offering a viable alternative to the conventional hydrotreatment process.

1.1. Objectives

The main objective of this work is the synthesis of metallic nanoparticles and their coating with silica and carbon for application in denitrogenation processes. Specific objectives include:

- Extensive characterization of the materials (textural properties, Fourier transform infrared spectroscopy, contact angle, among others).
- Application of the materials in ODN with hydrogen peroxide as the oxidant.

- Comparison of the coating swith silica and with carbon in the removal of quinoline.

- Evaluation of the adsorptive capacity of the materials.

1.2. Report Outline

This MSc dissertation is divided into 6 chapters, including the present one, where the motivation to study alternatives to the removal of nitrogen-containing compounds from fossil fuels, the main objectives to be achieved, and the proposed structure to present and discuss the research are outlined.

The second chapter addresses the fundamental aspects of fossil fuels and their environmental impact, treatments for the removal of nitrogen-containing compounds, the denitrogenation process with hydrogen peroxide in a biphasic system, and the role of cobalt ferrite-based catalysts, including those with carbon and silica coatings.

In chapter 3, the chemicals, materials, and synthesis procedures, along with the equipment and experimental methodologies used in this study, are described in detail. Chapter 4 presents and discusses the experimental results, including catalyst characterization, quinoline removal efficiencies, H_2O_2 decomposition studies, and insights from degradation pathways and intermediate analyses.

Finally, in chapter 5, the main conclusions of this thesis are summarized. Suggestions for future work are provided in chapter 6, to optimize and expand upon the studies presented in this dissertation.

STATE OF THE ART

2. STATE OF THE ART

2.1. Fossil Fuels

From its initial conception to its current fundamental role as an indispensable component for production and economic progress, energy remains an indispensable resource throughout the world. The search for energy is expected to triple by the end of the 21st century compared to its beginning, signaling not only the constant evolution of energy demands, but also the growing interdependence between energy and contemporary challenges [1].

In 2022, global primary energy consumption increased by 3% compared to the pre-COVID 2019 level. Oil-based fuels remained the main source of energy, accounting for 82% of total consumption [2]. Over the last 20 years, oil demand has seen a remarkable increase of 18 million barrels per day. This significant growth is largely attributable to increased consumption in road transportation, which has expanded its activity by almost 65% during this period and currently constitutes approximately 45% of global oil demand [3].

However, during combustion, fossil fuels, which predominantly consist of carbon and hydrogen, as well as sulfur, nitrogen and oxygen, generate gaseous by-products such as oxides of carbon (CO and CO_2), nitrogen (NOx) and sulfur (SOx). These by-products trigger both impacts on engines, such as incomplete combustion, particle formation and deposition and engine corrosion, and a series of environmental impacts, since these substances are classified as greenhouse gases, contributing significantly to global warming and atmospheric pollution [4].

Globally, nine out of ten people face exposure to air pollutants, making air pollution one of the main environmental challenges and a significant threat to human health. This translates into more than 6 million premature deaths annually, with approximately 73% of these fatalities being attributed to the inhalation of ambient air contaminated by polluting sources such as vehicle and industrial emissions [3].

Although fossil fuels have shown stability in total energy consumption in recent years, there has been an increase in the share of renewable energies, which now account for 7.5% of the global energy matrix, a scenario that shows the gradual shift towards more

sustainable sources with lower environmental impacts, marking a significant advance in the global energy panorama [2].

Faced with the transformation in the global energy outlook and the growing need to comply with stricter environmental regulations, it is becoming essential to develop technologies that improve the quality of fossil fuels and reduce the emission of harmful by-products. During oil processing, techniques such as catalytic treatment and the oxidative removal of contaminating compounds play significant roles in improving fuel quality, while at the same time contributing to compliance with these regulations [4].

2.2. Nitrogen in Fossil Fuels

Crude oil is rich in a variety of nitrogen compounds, especially molecules containing a single nitrogen atom (N_1), mainly aromatic compounds and, to a lesser extent, aliphatic compounds such as amines and nitriles [11]. These predominant compounds can be divided into two main categories: the basic, or pyridinic, exemplified by substances such as pyridine and quinoline, and the non-basic, or pyrrolic, represented by compounds such as pyrrole, indole and carbozole, as illustrated in Figure 1 [5].

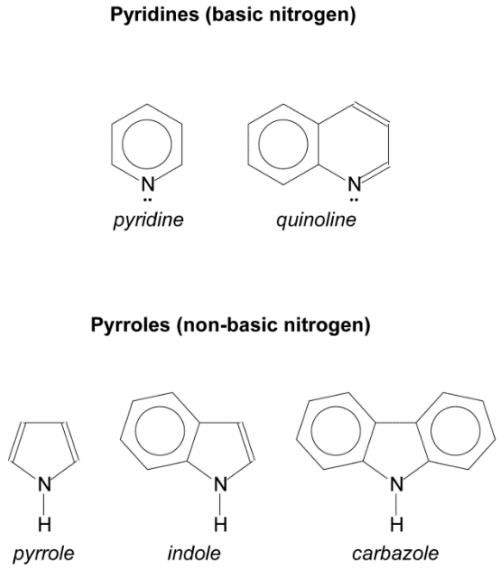

Figure 1. Examples of nitrogen compounds present in fossil fuels [5].

Despite making up a modest fraction, ranging from 0.1 to 1.5%, in the composition of fossil fuels [4], the removal of nitrogen compounds is an imperative need, since they not only trigger environmental concerns due to the emission of NOx when

burning fuels, but also cause adverse impacts on the oil refining process and fuel quality, notably by affecting the removal of other contaminants [5].

Pyrrolic compounds are prone to free radical addition reactions, resulting in the unwanted formation of gums, presenting a significant challenge due to their insoluble properties and ability to cause fouling and deposits on industrial equipment. On the other hand, basic compounds derived from pyridine can react with acids present in the oil, generating salts, precipitating and contributing to fouling in equipment, introducing additional challenges in the industrial processing of oil [5].

In catalytic processes of contaminants removal, such as hydrotreating, nitrogen compounds compete for the active sites of the catalysts with other contaminants, such as sulfur, and can impair the efficiency of the process, limiting the access of other compounds to the active sites and potentially poisoning the catalysts. The steric effect, especially in nitrogen compounds with bulky groups or complex three-dimensional structures attached to the nitrogen atom, further accentuates this challenge [6].

In addition, the superior thermal stability of nitrogen compounds, derived from stronger and shorter covalent bonds, makes them more resistant to breakage compared to sulfur compounds. This same thermal stability also contributes to the difficulty in removing nitrogen compounds during refining processes, due to their lower reactivity and greater chemical stability, factors that increase the resistance of nitrogen to removal [9].

2.3. Legislation

Despite the various impacts caused by the presence of nitrogen in fuels, fuel specifications only indirectly regulate nitrogen content, focusing on controlling gum content, storage stability and thermal stability [5].

However, Europe sets strict criteria for vehicle emissions through the EURO standards, which have been adapted to emission levels and the development of pollutant reduction technologies over the years. In force since 2014, Euro 6/VI has reduced NOx emissions by 22% for light vehicles, such as cars and vans, and 36% for trucks and buses on European roads, by determining that vehicles certified by the standard should be equipped with advanced emission control technologies, such as exhaust gas recirculation (EGR) systems, particulate filters (DPF) and selective catalysts for NOx reduction (SCR), minimizing the release of pollutants during combustion in diesel and gasoline engines [7].

Euro 7, scheduled to come into force in 2025, is a proposal that replaces and unifies regulations that, in the current Euro standard, vary for passenger cars and commercial vehicles (Euro 6), and trucks and buses (Euro VI), defining emission limits for all vehicles in a single set of rules. In addition, Euro 7 reduces the pollutant emission limits for heavy-duty vehicles and standardizes the low limits for light-duty vehicles, regardless of the type of fuel used, whether petrol, diesel or other [8].

The new standard also introduces emission limits for previously unregulated pollutants, such as nitrous oxide emissions (N_2O) from heavy-duty vehicles, as well as doubling Euro 6/VI's low-emission vehicle durability requirements by stipulating that every vehicle must comply with the low-emission rules until it reaches 200,000 kilometers and 10 years of age, and aims to ensure that vehicles within the standard have pollutant emissions easily controlled from sensors inside the vehicle. Through these changes, Euro 7 projects a significant reduction in NOx emissions by 2035, achieving a reduction of 85% in light vehicles and 80% in heavy vehicles, compared to 2018 levels [8].

Therefore, even though the regulation of nitrogen is much more focused on emissions, it is clear that there is a need to study processes specifically focused on its removal.

2.4. Ways of Removing Nitrogen from Fossil Fuels

Various methods have been explored for the denitrogenation of fuels, such as catalytic hydrotreatment (HDN), oxidation (ODN), extraction (EDN), adsorption (ADN) and biological denitrogenation (BDN) [13]. However, the effectiveness of the process can vary according to the nitrogen content in the oil, making the selection of the most appropriate technique for oils with a high nitrogen content a considerable challenge [9].

Some techniques require specific conditions and strict control of parameters and are most commonly used to remove nitrogen from oils with a low content of this element (<0.1% by mass of N). These techniques include: (i) microbial conversion, which uses microorganisms to degrade the nitrogen in the oil; (ii) methods that require precise control of chemical reactions, such as alkylation and hydrolysis, followed by separation of the nitrogen by extraction, distillation or filtration; (iii) liquid-liquid extraction, based on the difference in solubility between nitrogen and the solvent, requiring prolonged post-

treatment to recover the solvent; (iv) adsorption, which makes use of highly nitrogen-selective adsorbents, requiring regeneration in each cycle [5].

Hydrotreatment is the most widely used technique industrially, as it is a catalytic process capable of simultaneously reducing unwanted compounds such as metals and sulfur, nitrogen and oxygen compounds. The selection of the catalyst plays a crucial role in this process, and it is common industrially to use molybdenum and tungsten sulphides supported on alumina, modified by cobalt for greater sulfur selectivity, while nickel is more selective for nitrogen removal. In addition, the reaction conditions, including the amount of H_2, pressure, temperature and the presence of impurities, have a strong influence on the results obtained [9].

The elimination of nitrogenous compounds from the oil, both basic and non-basic, takes place through the hydrogenation of aromatic rings forming reactive intermediates, followed by ring opening and denitrogenation [9]. Figure 2 illustrates the process of hydrogenation of pyridine to piperidine, subsequent transformation into pentylamine and, finally, elimination of NH_3 to produce pentane.

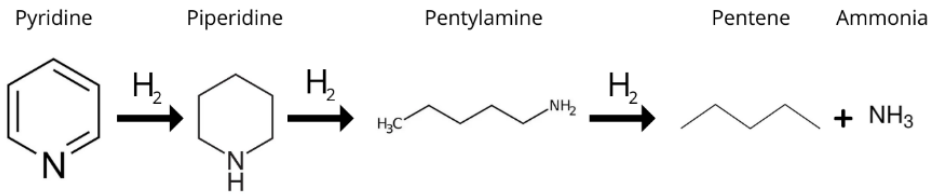

Figure 2. Pyridine hydrogenation process [9].

During hydrodenitrogenation (HDN), the removal of aromatic nitrogen is comparatively more complex than that of aliphatic nitrogen, since it requires saturation of the ring before denitrogenation. This need makes hydrotreating an even more expensive technique, not only because of the high hydrogen pressure, but also because of its high consumption [11].

In addition, effective HDN, combined with the simultaneous removal of other impurities, presents unique challenges due to the strong affinity of nitrogen compounds for the catalyst's active sites. Although these compounds exhibit lower reaction rates compared to sulfur compounds, their more intense interaction with the catalyst results in higher adsorption constants, hindering the removal of other impurities and potentially

poisoning the catalyst [9]. Considering the high hydrogen consumption, the catalyst challenges and the demands for higher temperatures (260-425°C) and substantial pressures (5-160 bar), hydrotreating is recognized as an operationally costly process [12]. Therefore, the search for alternatives for nitrogen removal is essential.

2.5. Oxidative Denitrogenation

Oxidative denitrogenation (ODN) can play a dual role in the fuel refining process. In addition to complement hydrotreating, it provides an additional approach to remove nitrogen contaminants prior to the process, especially when ammonia, a common by-product of hydrodenitrogenation, may compromise the catalyst used in hydrodesulfurization (HDS), thus improving the overall efficiency of the process. It can also be an alternative to HDN, being potentially more effective or economical in certain situations or for certain types of fuels, as an independent route for nitrogen removal, highlighting its versatility in the context of fuel refinement [14].

Oxidation of impurities represents a highly promising route in fuel refinement, often mentioned in literature [16-19] as a viable alternative, especially in relation to hydrodesulfurization. Although they occur simultaneously, denitrogenation has received less attention than desulfurization. This can be attributed, in part, to the history of regulations limiting the amount of sulfur in fuels, due to the serious environmental impacts associated with this compound, which are proportionally greater than those caused by nitrogen compounds, as well as nitrogen's resistance to removal compared to sulfur, as mentioned above. Consequently, there has been more significant investment in desulfurization techniques over the years, while denitrogenation has remained relatively less explored and less developed [15].

With its milder temperature and pressure conditions, between 25 and 140°C and 1 to 2 bar, respectively, than hydrotreating, oxidation eliminates the need for specialized reactors for extreme conditions, and potentially preserves the integrity of the olefins and maintains essential fuel parameters, such as octane rating. One of the main approaches in oxidation processes is done in two stages: oxidation and subsequent extraction or adsorption of the oxidized compounds. Oxidation is a technique that results in a wide range of reaction products due to the large number of bonds in nitrogen compounds that are susceptible to oxidation [12].

The resulting oxidized compounds have a significantly higher polarity than the original compounds, facilitating their extraction [13]. Various oxidants, such as hydrogen peroxide, organic peracids, oxygen and ozone, are used in the process to trigger the oxidation of nitrogen compounds, and the removal of oxidized compounds can be done by adsorption, but is mainly carried out through liquid-liquid extraction, using a variety of solvents, such as acetonitrile (ACN), carbon tetrachloride (CCl_4), ethanol (EtOH), methanol (MeOH), ionic liquids (IL), among others. Aqueous phases containing hydrogen peroxide, as well as an oxidizer, can also act as an extraction phase [12].

Hydrogen peroxide (H_2O_2) is a versatile compound, widely used in various applications due to its properties as a highly effective oxidizing agent. With global production exceeding 5 million tons annually, its stability, ease of handling and ability to release active oxygen set it apart from other oxidizing compounds and make it particularly valuable in the oxidation of a variety of compounds, including nitrogen compounds [20].

Although reagents such as H_2O_2 or other oxidizing agents are effective against contaminants such as sulfur and nitrogen, a significant challenge arises: their solubility in polar solvents. This becomes especially problematic considering that fuels contaminated by these elements are in a non-polar oily phase, resulting in a two-phase liquid system [21]. This configuration limits mass transfer at the two-phase interfaces during oxidation, which ultimately reduces the overall rate of the oxidative reaction. However, a promising solution to these challenges is the development of amphiphilic metal catalysts, which are modified with hydrophobic and hydrophilic regions, offering new perspectives on biphasic systems and improving ODN performance [22].

2.6. Isooctane and Quinoline

A crucial component of gasoline, isooctane (iC_8) is less complex than the mixture of hydrocarbons that make up this fuel. Due to its relatively well understood oxidation chemistry, isooctane is often chosen as a model compound to represent gasoline in scientific studies [32].

On the other hand, the presence of quinoline (C_9H_7N), one of the basic nitrogen compounds found in crude oil, is a constant concern due to its toxicity, carcinogenic potential and relative solubility in water. Quinoline (QN), in addition to the impacts already mentioned in relation to nitrogen compounds in fuels, is also commonly found in

pharmaceutical wastewater due to its application in certain pharmaceutical products. Therefore, its removal is an important issue that can be tackled through various methods, including biodegradation, photodegradation, hydrotreatment and oxidation [33].

The process of removing quinoline by hydrotreating is complex and involves several steps. Initially, the polycyclic ring is hydrogenated, followed by the hydrogenation of a phenyl ring and the cleavage of the carbon-nitrogen bond to remove nitrogen, resulting in less harmful compounds. This process has several routes and requires a high consumption of hydrogen [9]. Figure 3 illustrates the possible routes that hydrodenitrogenation of quinoline can follow.

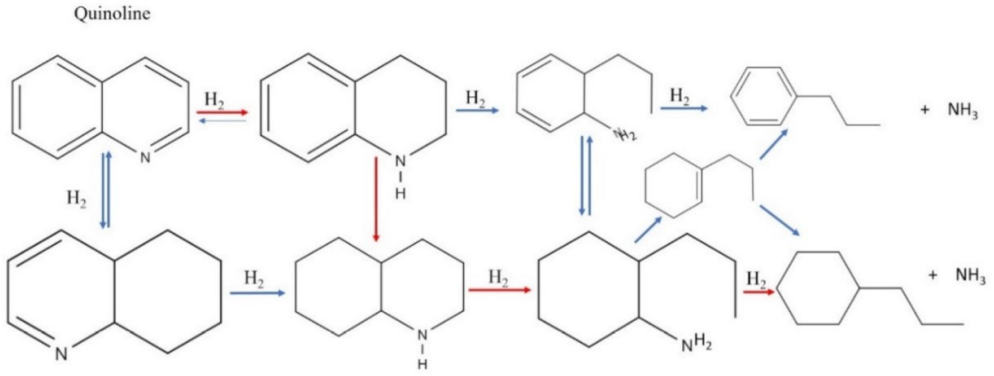

Figure 3. Quinoline hydrogenation process [9].

The oxidation of quinoline is a process that generates several reaction intermediates, since various elements of the molecule are susceptible to chemical reactions [14]. The main products are 5-hydroxyquinoline and 8-hydroxyquinoline, and some trace amounts of 3-, 6- and 7-hydroxyquinoline can also be observed [12]. Such trends in product formation may be due to the electronic density mapping of quinoline, which revealed that positions 2, 4, 5 and 7 are susceptible to nucleophilic attack, while positions 1, 3, 6 and 8 are more prone to electrophilic attack [14], providing fundamental insights into the sites of reactivity of this molecule, as shown in Figure 4.

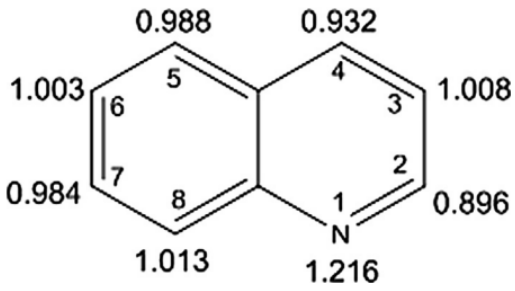

Figure 4. Electronic density of quinoline [14].

Understanding the reactivity of quinoline is crucial for the optimization of oxidation processes and the selective synthesis of specific products. Several experimental conditions have been investigated in previous studies for the removal of quinoline by oxidation [14, 34-39], using different catalysts, oxidants, extractants and reaction parameters. These approaches demonstrated significant rates of conversion and removal of quinoline, as shown in Table 1.

Table 1. Examples of experimental conditions for ODN found in the literature.

Ref.	Technique and compound removed	Catalyst	Oxidizer	Extractor	Reaction conditions	Results
[14]	Oxidative Denitrogenation (ODN) - Quinoline	Vanadium Oxide (V_2O_5) Supported on Silica (SiO_2)	Terc-Butyl-Hydroperoxide (t-BuOOH)	2,6-Pyridine-Polybenzimidazole (2,6-PyPBI) nanofibers	70° C, 12 hours, 7:1 Oxidizer:Substrate ratio	78% total conversion of QN; 67% selectivity and 86% removal for QN-N-Oxide;
[34]	Catalytic Aerobic Oxidation (ODN) - Indol and Quinoline	Porous Carbon Co-Doped with Oxygen and Phosphorus (PPDC)	Molecular Oxygen (O_2)	Ethyl Acetate $C_4H_8O_2$	100 °C, 4 hours, 30 mg catalyst, 50 mL/min O_2, 500 ppm Indol or Quinoline	IND conversion: 95% and QN: 86%, Catalyst recyclability
[35]	Extractive Catalytic Oxidative Denitrogenation (ECODN) - Quinoline	Vanadium-substituted Dawson's salt ($[Cetrimonium]_{11}P_2W_{13}V_5O_{62}$)	Hydrogen Peroxide (H_2O_2)	Ionic liquid 1-butyl-3-methyl imidazolium methyl sulfate ($[Bmim]mSO_4$)	70 °C, 45 min, 1:8 ratio of Ionic Liquid:Oil, 7.5 g/L of Catalyst	Removal of 94% of S and 100% of QN, Stable and Recyclable Catalyst

Table 1-cont.. Examples of experimental conditions for ODN found in the literature.

Ref.	Technique and compound removed	Catalyst	Oxidizer	Extractor	Reaction conditions	Results
[36]	Selective Oxidation followed by Ionic Liquid Extraction (ODN-ILs) - Quinoline	Vanadium complex linked to the diphenylamine salt debis(salicylaldehyde) ([VO(salt-HBPD)])	Hydrogen Peroxide (H_2O_2)	Imidazoline-based Ionic Liquid	50 °C, 30 min, 300 rpm, ratio 1:7 Quinoline:H_2O_2	Oxidation Produces QN-N-Oxide, Extraction of 96% and 87% with Ionic Liquids
[37]	Extractive Catalytic Oxidative Denitrogenation (ECODN) - Quinoline	Vanadium Complex (PWV5) in Silica with Tri-Methyl-Propyl Ammonium Groups (TMA-Si)	Hydrogen Peroxide (H_2O_2)	Acetonitrile	70 °C, ratio 4:1 Oxidizer:Oxidizing Agent, ratio 1:6 Solvent:Oil Volume, 7.5 g/L Catalyst	100% QN removal, 95% S, Catalyst recyclability
[38]	Catalytic Extraction and Oxidation (ECODN) - Quinoline and Indol	Polyoxometalate incorporated into metal-organic framework PMo_{12}@MIL-100(Fe)	Hydrogen Peroxide (H_2O_2)	Ionic Liquid [BMIM]PF_6, Ethanol (EtOH)	70 ºC, 30 min, 1:1 Fuel Model:Solvent Extractor	Complete Removal of S and N with Recyclability of Catalyst and EtOH Solvent
[39]	Oxidation Denitrogenation (ODN) - Quinoline	None	Ascorbic Acid ($AscH_2$), Hydrogen Peroxide (H_2O_2)	None	30 °C, Contact time 30 min	98.8% QN removal

2.7. Catalysts for Oxidation Processes

The presence of efficient catalysts plays a crucial role in the oxidation stage and is fundamental to the success of ODN [21]. For the successful industrial implementation of these oxidative processes, substantial achievements are needed in the development of highly active and selective catalysts for oxidation [19].

Efficient catalysts for the oxidation process share fundamental characteristics. They must exhibit high catalytic activity, driving the reaction and allowing high conversions of the contaminant. In addition, it is essential that they have the ability to efficiently exchange electrons, facilitating the transfer of electrons between the reactants,

the catalyst and the oxidizing agent, promoting the formation of active oxygen species and the oxidation of contaminants. Catalytic stability is another crucial characteristic, as the catalyst must maintain its activity and structure intact over prolonged reaction periods, resisting deactivation, sintering or poisoning by intermediates or by-products. Finally, catalytic selectivity is indispensable, ensuring that the reaction is directed towards the desired products, minimizing the formation of unwanted or toxic by-products [40, 41].

A typical solid metal catalyst for these purposes comprises an active phase, such as transition metals (Fe, Ni, Co), supported on a highly stable material. Iron species, for example, exhibit magnetic properties and can be easily removed from the reaction, facilitating phase separation after the oxidation process. This attribute allows the materials to be attracted by an external magnetic field, breaking the emulsion and facilitating phase separation, as well as allowing the catalysts to be reused in subsequent reactions [21].

Ferrite nanoparticles can have different crystal structures. Cobalt ferrite ($CoFe_2O_4$), for example, has an inverse spinel structure and is of great interest due to its unique electrical, magnetic and catalytic properties compared to its bulk counterparts. In its cubic arrangement of atoms Fe^{3+} ions occupy the A and B sites, while all Co^{2+} ions are in the B sites, as shown in Figure 5, giving to cobalt ferrite exceptional electromagnetic performance, excellent chemical stability, mechanical hardness, high coercivity and moderate saturation magnetization [25].

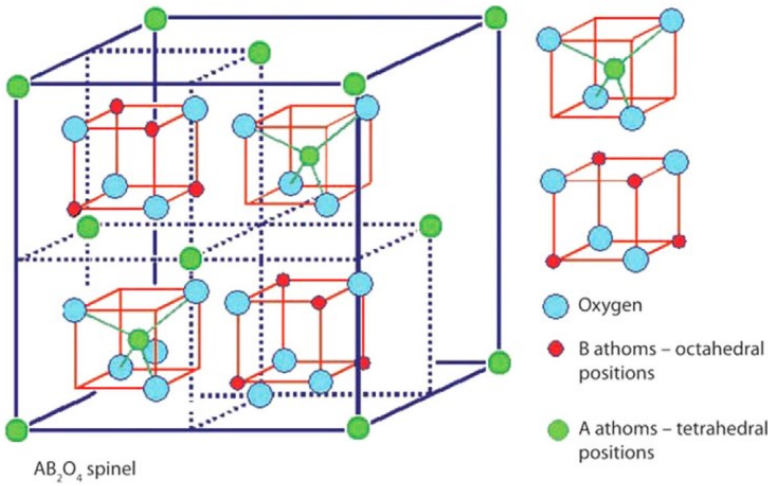

Figure 5. Spinel structure of cobalt ferrite [26].

The structural characteristics of cobalt ferrite are fundamental to improve its performance as a catalyst in oxidation processes, giving the ferrite high chemical stability, promoting its efficiency and durability during oxidation reactions. The orderly arrangement of the atoms in the spinel structure of cobalt ferrite allows for precise interaction with the reagents, favoring the chemical transformations necessary for the oxidation of contaminants, such as nitrogen compounds, in various industrial and environmental contexts [29].

Various procedures are used in the synthesis of cobalt ferrite nanoparticles, including the sol-gel method, hydrothermal, microemulsion, aqueous precipitation, polyol and combustion. Each technique has its advantages and limitations, but the sol-gel method stands out for its versatility and precise control over the composition and morphology of the nanoparticles [25].

The sol-gel method is a chemical technique used to produce inorganic materials from liquid precursors. It consists of forming a gel from the hydrolysis and polycondensation of inorganic precursors, followed by drying and calcination to form the final material. This process offers the advantage of controlling the material's properties, such as particle size, porosity and chemical composition, making it a powerful approach in the synthesis of spinel cobalt ferrite nanoparticles [30].

The search for nanomaterials with controlled morphologies and adapted properties has been a priority in the scientific community [23]. These advances aim not only to optimize process performance, but also to reduce the disposal of materials such as catalysts. The coating of nanoparticles has emerged as an important strategy in this scenario, providing stability to the particles and protecting them from degradation during the reaction time. It is essential to guarantee the stability of the catalysts, because during operations there is a risk of metal particles being released into the liquid medium [24].

Coating magnetic nanoparticles can broaden their potential applications, including catalysis, adsorption, controlled drug release and magnetic therapy. By coating the cobalt ferrite, the aim is to ensure greater stability for the material, protecting its metallic core from physical and chemical changes during chemical reactions such as oxidations. In addition, the coating can improve the adsorptive capacity of the cobalt ferrite, creating catalytic active sites by depositing the coating material on the particles.

These characteristics make coating an important strategy for optimizing the performance and durability of nanoparticles in various technological and biomedical applications [29].

There are several approaches to produce magnetic nanocomposites, including monodisperse magnetic nanocrystals embedded in mesoporous nanospheres, microspheres encapsulating magnetic cores, and mesoporous materials loaded with magnetic nanoparticles. These techniques provide a variety of options for the design and application of these materials in different contexts [23].

2.8. Coating

As mentioned above, a variety of materials can be used to coat metal cores, giving to the metal catalysts specific characteristics and properties.

Metal catalysts can undergo surface modifications that result in the generation of active species when coated with materials such as polymers, silica, carbon and other compounds, capable of transforming them into hybrid materials. Due to their amphiphilic nature, simultaneous interactions with aqueous and oily phases are possible, so these hybrid materials play a significant role in two-phase reactions. This property promotes an increase in the interface between the phases, facilitating the formation of a stable emulsion during the two-phases process [21].

Carbon-based materials, for example, have the ability to generate oxidizing species from oxidizing sources, such as hydroxyl radicals from hydrogen peroxide [12]. These materials can be synthesized in a variety of ways, including hydrothermal carbonization, chemical vapor deposition and methods such as modified Stöber and resorcinol-formaldehyde (RF) polymerization. The latter method is often chosen because it provides optimum performance in applications such as adsorption, ultrafiltration and catalysis, due to the deposition of the polymer on the surface of the metal core [27].

Silica coating, in turn, can affect the adsorption capacity of certain contaminants [28]. In addition, silica plays an essential protective role, preventing physical and chemical alterations to the magnetic core, including secondary reactions. A multi-layer approach is generally employed, where silica is coated with another additional material [29]. To carry out this silica coating, the Stöber method is often used, mainly using tetraethylorthosilicate (TEOS). In this process, the hydrolysis products are condensed in a polar mixture, such as ethanol/water, in a basic medium [30].

The combination of silica-carbon coating is also possible and can generate Janus particles, anisotropic functional particles made up of two types of surface with different physical-chemical properties spatially isolated [31].

MATERIALS AND METHODS

3. MATERIALS AND METHODS

3.1. Reactants and Equipaments

The reagents used in this work are given below, distributed according to each experiment in which they were used.

3.1.1. Synthesis of the Superparamagnetic Core ($CoFe_2O_4$)

- Cobalt(II) nitrate hexahydrate (99%), Fisher Scientific. Formula: $Co(NO_3)_2 \cdot 6H_2O$;
- Iron(III) nitrate nonahydrate (98%), Merck. Formula: $Fe(NO_3)_3 \cdot 9H_2O$;
- Ethylene glycol (99.5%), Fluka Analytical. Formula: $C_2H_6O_2$;
- Acetone, Fisher Scientific. Formula: C_3H_6O;
- Absolute Ethanol (99.8%), Fisher Scientific. Formula: C_2H_5OH.

3.1.2. Synthesis of $CoFe_2O_4$@SiO_2

- Magnetic core ($CoFe_2O_4$) previously synthesized;
- Distilled Water;
- Absolute Ethanol (99.8%), Fisher Scientific. Formula: C_2H_5OH;
- Ammonia solution (28%), Supelco. Formula: NH_3;
- Tetraethyl orthosilicate (TEOS) (98%), ThermoScientific. Formula: $Si(OC_2H_5)_4$.

3.1.3. Synthesis of $CoFe_2O_4$@C

- Magnetic core ($CoFe_2O_4$) previously synthesized;
- Distilled Water;
- Absolute Ethanol (99.8%), Fisher Scientific. Formula: C_2H_5OH;
- Ammonia solution (28%), Supelco. Formula: NH_3;
- Resorcinol (99%), Alfa Aesar. Formula: $C_6H_4(OH)_2$;
- Formaldehyde (37% stabilized with methanol), Panreac. Formula: CH_2O.

3.1.4. Adsorption and Oxidation Reactions

- 2,2,4-Trimethylpentane (isooctane), Fisher Scientific. Formula: C_8H_{18};
- Quinoline (98%), Alfa Aesar. Formula: C_9H_7N;
- Hydrogen peroxide (60%), Fisher Scientific. Formula: H_2O_2 (for oxidation reactions)

- Catalysts: metallic core, carbon-coated core and silica-coated core.

3.1.4.1. High-Performance Liquid Chromatography (HPLC)

Reagents for the preparation of buffer solutions and calibration curves to analyze the concentration of quinoline by HPLC:

- Ultrapure water;
- Acetonitrile (99.9%), Fisher Chemical, Formula: C_2H_3N;
- Ammonium acetate, VWR Chemicals, Formula: CH_3COONH_4.

3.1.4.2. UV-VIS Chromatography

Reagents for the preparation of calibration curves to analyze the quantity of hydrogen peroxide and quinoline:

- Titanium (IV) oxysulfate solution, Sigma-Aldrich, Formula: $TiOSO_4$;
- Sulfuric acid (98%), Labkem, Formula: H_2SO_4;
- Ethanol Absolute (99.8%), Fisher Scientific. Formula: C_2H_5OH.

3.1.4.3. Gas Chromatography

- N-hexadecane in cyclohexane solution (1 mg/mL)

3.1.5. Equipaments

The methodology involved various specialized equipment and techniques to synthesize, characterize and apply the superparamagnetic cobalt ferrite ($CoFe_2O_4$). Some of the main pieces of equipment are: magnetic stirrer, muffle furnace, magnet, vertical tube furnace, pH meter, ultrasonic bath, PANalytical X'Pert PRO diffractometer, Perkin Elmer FTIR spectrophotometer, Quantachrome NOVA TOUCH LX4 analyzer, high-performance liquid chromatography (HPLC) equipped with a UV-VIS detector (UV-2075 Plus), UV-VIS spectrophotometry (Jasco V-530), gas chromatography with flame ionization detection (GC-FID) and mass spectrometry (GC-MS) and a SHIMADZU TOC-L analyzer, as well as glassware and other tools such as pipettes and spatulas. Each piece of equipment was essential to ensure accurate synthesis, characterization and analysis throughout the research process.

3.2. Methodology

3.2.1. Synthesis of the Superparamagnetic Core ($CoFe_2O_4$)

The synthesis of the superparamagnetic cobalt ferrite ($CoFe_2O_4$) core was performed using the sol-gel method previously adopted by the group [30].

First, 4.76 g of cobalt(II) nitrate hexahydrate ($Co(NO_3)_2 \cdot 6H_2O$) was dissolved in 20 mL of ethanol (C_2H_5OH). This solution was heated under magnetic stirring until it reached the boiling point, and then cooled in an ice bath until thermal equilibrium at room temperature (20 °C) was reached. Subsequently, 10.83 g of iron(III) nitrate nonahydrate ($Fe(NO_3)_3 \cdot 9H_2O$) was dissolved in 80 mL of ethylene glycol ($C_2H_6O_2$). This solution was heated under magnetic stirring for 5 minutes at 60 °C and then cooled in an ice bath until thermal equilibrium was reached.

Once both solutions reached thermal equilibrium, they were combined in a single 250 mL beaker and warmed at 60 °C for 2 hours under continuous stirring. The temperature was then increased to 120 °C and maintained until a gel formed. Afterwards, the temperature was further increased to 189 °C to evaporate the solvent, turning the gel into a solid.

The solid material obtained was transferred to a crucible and heated in a muffle furnace at 600 °C for 12 hours with a heating rate of 1 °C/min to calcine and remove any organic impurities. After the thermal treatment, the magnetic core was washed several times with acetone (C_3H_6O) and ethanol (C_2H_5OH) to remove any unreacted excess reagents. The solution initially turned blue, indicating the presence of residual compounds, and washing continued until the solution became clear. A magnet was used to efficiently separate the magnetic particles from the liquid, as they were easily attracted to it, as shown in Figure 6. The cleaned material was then dried in oven at 60 °C for 24 hours.

Figure 6. Metallic particles attracted by a magnet.

3.2.2. Synthesis of $CoFe_2O_4$@SiO_2

The coating process followed a methodology adapted from Liu et al. [23]. First, 0.25 g of the cobalt ferrite was suspended in a mixture of 50 mL of distilled water and 150 mL of ethanol with the aid of an ultrasonic bath to disperse the nanoparticles. The suspension was then transferred to a 500 mL two-necked round bottom flask, and 3.9 mL of ammonia reagent (28%) was added. This mixture was stirred at 30 °C for 1 hour to ensure proper dispersion of reactants. After this period, 0.41 mL of TEOS were added to the mixture to start the condensation reaction.

The reaction mixture was maintained at the same temperature and stirring conditions for 6 hours, then the temperature was raised to 50 °C and maintained for another 12 hours. Upon completion, the final solid was recovered from the mixture and washed several times with distilled water until the rinse waters reached neutral pH. The washing process was facilitated by using a neodymium magnet to recover the magnetic nanoparticles from the liquid media.

The recovered particles were annealed in inert atmosphere at 600 °C, using a heating ramp of 120 °C/min, in a vertical tubular furnace under a nitrogen (N_2) flow of 100 Ncm^3/min, resulting in $CoFe_2O_4$@SiO_2.

3.2.3. Synthesis of $CoFe_2O_4$@C

The synthesis process for $CoFe_2O_4$@C followed the same steps as for $CoFe_2O_4$@SiO_2, with the key differences being the absence of TEOS and the addition of resorcinol and formaldehyde [23].

0.25 g of the cobalt ferrite core was suspended in a mixture of 50 mL of distilled water and 150 mL of ethanol with the aid of an ultrasonic bath to disperse the nanoparticles. The suspension was then transferred to a 500 mL two-necked round bottom flask, and 3.9 mL of ammonia reagent (28%) and 0.2 g of resorcinol were added. This mixture was stirred at 30 °C for 1 hour to ensure proper dispersion of reactants. After this period, 0.3 mL of formaldehyde was added to the mixture to start the polymerization reaction of resorcinol and formaldehyde (RF).

The reaction mixture was maintained at the same temperature and stirring conditions for 6 hours, then the temperature was raised to 50 °C and maintained for another 12 hours. Upon completion, the final solid was recovered from the mixture and washed several times with distilled water until the rinse waters reached neutral pH. The washing process was facilitated by using a neodymium magnet to recover the magnetic nanoparticles from the liquid media.

The recovered particles were annealed in inert atmosphere at 600 °C, using a heating ramp of 120 °C/min, in a vertical tubular furnace under a nitrogen (N_2) flow of 100 Ncm^3/min, resulting in $CoFe_2O_4$@C.

3.2.4. Adsorption and Oxidation Runs of Quinoline

3.2.4.1. Adsorption Runs

The adsorption runs were conducted in a two-phase system with an organic-to-aqueous phase ratio of 80:20. The organic phase consisted of 40 mL of isooctane containing quinoline at a concentration of 1 g/L, and the aqueous phase comprised 10 mL of distilled water adjusted to a pH of 3. These components were placed in a 100 mL reaction flask, to which 50 mg of adsorbent was added. The mixture was heated to 80°C on a magnetic hotplate equipped with a condenser, and continuous stirring was provided using a magnetic stir bar. This experiment was performed separately for three different materials: the uncoated metallic core, the carbon-coated core, and the silica-coated core.

To monitor the progress of the adsorption runs, samples of the organic and aqueous phases were taken proportionally at specific intervals during the reaction: 0, 15, 60, 120, 240 and 480 minutes. These samples were then analyzed to determine the adsorption efficiency of the catalysts.

3.2.4.2. Oxidation Reaction in Biphasic Medium

Non-catalytic oxidation reactions were carried out in a 250 mL reaction flask. Initially, 80 mL of isooctane containing quinoline (1 g/L) was heated to 80°C on a magnetic hotplate. Subsequently, 20 mL of aqueous phase adjusted to pH 3 was added, followed by 0.825 mL of hydrogen peroxide (60%). The reaction mixture was stirred continuously using a whisk under heating and samples were collected from both phases at specified intervals (0, 15, 30, 60, 120, 240, and 480 minutes).

Catalytic oxidation experiments followed a similar procedure to that used in non-catalytic oxidation, with an 80:20 organic-to-aqueous phase ratio, and maintained at 80°C. Initially, 80 mL of isooctane with quinoline (1 g/L) and 20 mL of aqueous phase adjusted to pH 3 were combined in a 250 mL flask. 0.825 mL of hydrogen peroxide (60%) was added, and after 2 minutes for phase stabilization, 100 mg of catalyst was introduced. The mixture was stirred continuously on a magnetic hotplate with a condenser at 80°C, as represented in Figure 7.

Figure 7. Set-up used in the oxidation experiments.

Samples were collected from both phases at specified intervals (0, 15, 30, 60, 120, 240, and 480 minutes). This procedure was repeated for three types of catalysts: uncoated metallic core, carbon-coated core, and silica-coated core.

3.2.5. Characterization Techniques

3.2.5.1. X-Ray Diffraction

X-ray diffraction (XRD) analysis was performed to investigate the phase composition and structure of the cobalt ferrite catalysts. The measurements were conducted using a PANalytical X'Pert PRO X-ray diffractometer equipped with an X'Celerator detector and a secondary monochromator (Cu Kα λ = 0.154 nm). Data were recorded at a step size of 0.017° over a 2θ angular range of 10–80°. The results were further processed using X'Pert HighScore Plus software for crystalline phase identification [47].

Also, the crystallite size of the synthesized cobalt ferrite was estimated using data from XRD analysis and the Size-Strain Plot (SSP) and Halder-Wagner methods [51]. In the SSP method, XRD peak broadening is assumed to be result from crystallite size and strain, modeled by combining Lorentzian and Gaussian profiles for size and strain effects, respectively. The total broadening, denoted as β_{hkl}, is related to the crystallite size D and deformation ε by the expression:

$$(d_{hkl} \cdot \beta_{hkl} \cdot \cos\theta)^2 = \frac{k\lambda}{D} \cdot (d^2{}_{hkl} \cdot \beta_{hkl} \cdot \cos\theta) + \frac{\varepsilon^2}{4}$$

where d_{hkl} is the interplanar spacing, θ is the Bragg angle and λ is the wavelength of the X-ray source (Cu Kα λ = 0.154 nm). A plot of $(d_{hkl} \cdot \beta_{hkl} \cdot \cos\theta)^2$ versus $(d^2{}_{hkl} \cdot \beta_{hkl} \cdot \cos\theta)$ was used to derive the crystallite size from the tilt and the intercept deformation.

The Halder-Wagner method similarly assigns the broadening to the crystallite size and strain, represented by a Voigt function. In this approach, the terms $\beta *_{hkl}$ and $d *_{hkl}$ were defined to simplify the calculation, leading to the equation:

$$(d *_{hkl} \cdot \beta *_{hkl})^2 = \frac{1}{D} \cdot (d *_{hkl} \cdot \beta *_{hkl}) + \varepsilon^2$$

A graph of $(d *_{hkl} \cdot \beta *_{hkl})^2$ versus $(d *_{hkl} \cdot \beta *_{hkl})$ provided the crystallite size from the slope and the deformation from the intercept.

3.2.5.2. Fourier Transform Infrared Spectroscopy

The Fourier Transform Infrared Spectroscopy (FTIR) analysis of $CoFe_2O_4$, $CoFe_2O_4$@C and $CoFe_2O_4$@SiO_2 were performed using a Perkin Elmer FTIR spectrophotometer in transmission mode. FTIR spectra were recorded in the wavenumber range of 450 to 4000 cm^{-1} with a resolution of 4 cm^{-1}. All measurements were obtained from the solid samples at room temperature, and the resulting spectra were obtained by Fourier transformation.

3.2.5.3. Textural Properties

The textural properties of the materials were characterized using nitrogen adsorption-desorption isotherms (N_2) at -196 °C (77 K) with a Quantachrome NOVA TOUCH LX4 adsorption analyzer, following the procedure outlined in previous group work [45].

Initially, the samples were weighed into glass cells and then degassed at 120 °C under vacuum conditions for 16 hours prior to measurement. This step was crucial for the removal of moisture and other volatiles, ensuring that the sample surfaces were clean and ready for accurate adsorption measurements.

The amount of nitrogen gas adsorbed by the samples was measured across various relative pressures (p/p_0). For surface area calculations, a relative pressure range of 0.05 to 0.35 was used, while the total pore volume was determined at a relative pressure of up to 0.98. These calculations were performed using the TouchWin™ v1.21 software, integrated into the Quantachrome NOVA TOUCH LX4 instrument.

.The specific surface area (S_{BET}) of the samples was determined using the Brunauer-Emmett-Teller (BET) method. The linear form of the BET equation is expressed as,

$$\frac{p/p_0}{n\,(1 - p/p_0)} = \frac{1}{n_m C} + \frac{C - 1}{n_m C}\,(p/p_0)$$

where p/p_0 is the relative pressure, n is the amount adsorbed, and n_m is the monolayer adsorption capacity.

The total pore volume (V_{Total}) was calculated from the amount of nitrogen adsorbed at a relative pressure of $p/p_0 = 0.98$, under the assumption that the pores are fully filled with liquid nitrogen at this pressure. The calculation is based on the density of liquid nitrogen (808,000 g/m³) and follows the formula,

$$V_{Total} = \frac{n \cdot M_{N_2}}{V_{N_2} \cdot \rho}$$

where M_{N_2} is the molar mass of N_2, V_{N_2} is the specific volume of N_2 and ρ is the density of liquid nitrogen.

Using the equipment, it was also possible to obtain the adsorption isotherms, allowing for their classification according to the 1985 IUPAC recommendations. This classification helps characterize the porous structure of the materials by identifying their type of isotherm and hysteresis loop. In them, physisorption isotherms are grouped into six types based on specific pore structures (as shown in Figure 8), while hysteresis loops are categorized into types H1, H2 (a and b), H3, H4, and H5, each related to distinct pore structure characteristics and adsorption mechanisms (illustrated in Figure 9) [46].

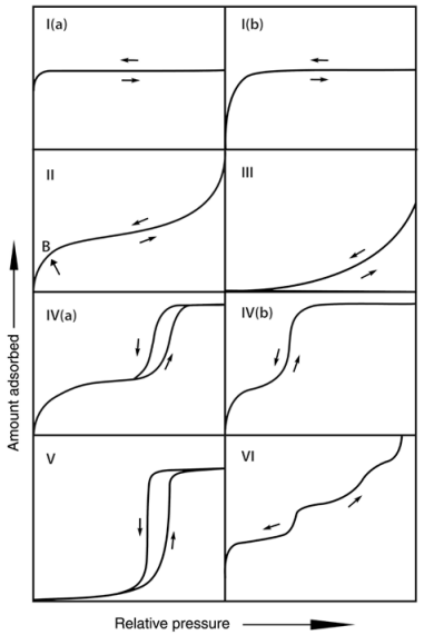

Figure 8. Classification of physisorption isotherms according to IUPAC [46].

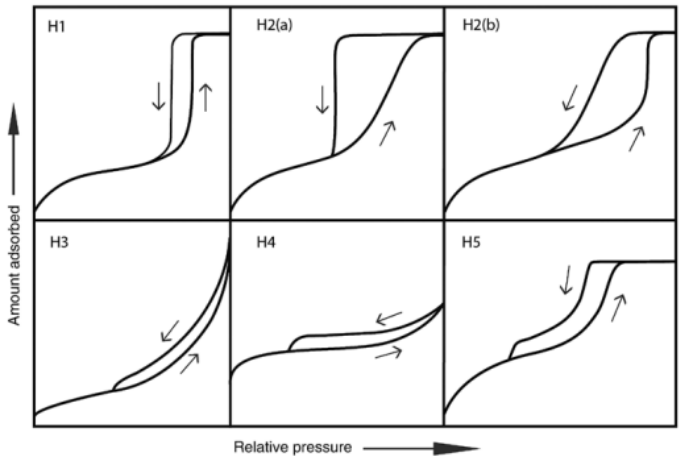

Figure 9. Classification of hysteresis loops according to IUPAC [46].

3.2.5.4. Contact Angle

The wettability of the surface of the cobalt ferrite materials was assessed by measuring the angle of contact with water using the sessile drop method. Each of the three materials was immobilized on a glass slide with the aid of a liquid adhesive, as reported elsewhere [43]. The glass slides-covered samples were dried overnight (60 °C) to remove moisture. Images of the droplets were captured with the aid of an Attension optical tensiometer (model theta) and analyzed with ImageJ software to determine the contact angle between the water and the material. The values are reported considering three measurements carried out in distinct parts of the glass slide.

3.2.6. Analytic Methods

3.2.6.1. High-performance liquid chromatography

To identify quinoline in the aqueous medium, a HPLC (High-performance liquid chromatography) was used, equipped with a UV-VIS detector (UV-2075 Plus), a quaternary gradient pump (PU-2089 Plus) for solvent delivery, and a column "NUCLEOSIL 100-5C18" (15 cm x 2.1 mm). A mobile phase consisting of 20% acetonitrile and 80% 10 mM sodium acetate solution was also used.

The buffer solution was prepared by dissolving 770 mg of ammonium acetate in 400 mL of ultrapure water, adjusting the pH to approximately 5.75 with 10% acetic acid, and then diluting to 1 L with ultrapure water. Subsequently, a 20% acetonitrile solution was prepared by mixing 200 mL of HPLC-grade acetonitrile with 800 mL of the prepared buffer solution. The solution was filtered using a 0.2 µm filter and a vacuum pump to remove any impurities and carefully transferred to a storage bottle to avoid forming bubbles.

Samples were prepared by mixing 100 µL of the aqueous phase with 900 µL of distilled water and injected manually into the chromatograph, samples from catalytic oxidation were previously filtered using a filter to prevent solids from being injected into the equipment. All analyses were performed in an isocratic system with a flow rate of 0.4 mL/min. Quinoline was detected at a wavelength of 313 nm.

3.2.6.2. UV-VIS chromatography

Adsorption of quinoline

Solutions of quinoline with varying concentrations (50, 40, 30, 20, 10, and 1 ppm) were prepared to create a calibration curve for analyzing quinoline concentration during the adsorption runs.

For the analysis, 0.15 mL of the aqueous and organic medium was collected and diluted with ethanol in a 5 mL volumetric flask. The samples were then analyzed by UV-VIS spectrophotometry (Jasco V-530) at a wavelength of 313 nm to measure absorbance.

Hydrogen concentration in aqueous phase

Hydrogen peroxide concentration was measured using a colorimetric method as reported in previous works [44].

Hydrogen peroxide solutions with various concentrations (30, 25, 20, 10, 5, 1, and 0.5 g/L) were prepared to obtain a calibration curve to follow the dissociation of hydrogen peroxide during the oxidation reactions of quinoline in biphasic systems with an initial concentration of 1 g/L of quinoline in the oily phase.

To determine the concentration of hydrogen peroxide (H_2O_2) during the oxidation process, 0.1 mL of the aqueous reaction medium was collected and diluted with distilled water in a 5 mL volumetric flask. Then, 0.8 mL of this solution was further diluted in a 10 mL volumetric flask containing 1 mL of sulfuric acid (H_2SO_4, 0.5 M) and 0.1 mL of titanium oxysulfate ($TiOSO_4$). Based on the formation of a yellow complex of hydrogen peroxide with titanium oxysulfate, the samples were analyzed by UV-VIS spectrophotometry (Jasco V-530) at a wavelength of 405 nm to measure absorbance.

3.2.6.3. Gas chromatography

The organic phase of the oxidation reactions was analyzed using gas chromatography with flame ionization detection (GC-FID) and mass spectrometry (GC-MS). Samples were prepared by diluting 0.6 mL of the organic phase, collected at 0, 15, 30, 60, 120, 240, and 480 minutes, with 0.1 mL of an internal standard solution of n-hexadecane in cyclohexane (1 mg/mL). To ensure the absence of solid materials, samples from the catalytic reactions were filtered using a filter before analysis.

3.2.6.4. Total Organic Carbon

Total Organic Carbon (TOC) analysis of liquid aliquots was performed using a SHIMADZU TOC-L analyzer. For the analysis, 0.2 mL of the sample was diluted to 20 mL in a volumetric flask.

RESULTS AND DISCUSSION

4. RESULTS AND DISCUSSION

4.1. Characterization Techniques

4.1.1. X-ray diffraction

Figure 10 shows the diffractogram obtained from the X-ray diffraction (XRD) analysis of the cobalt ferrite sample. The XRD analysis revealed a well-defined crystalline structure, with sharp diffraction peaks confirming the formation of cobalt ferrite.

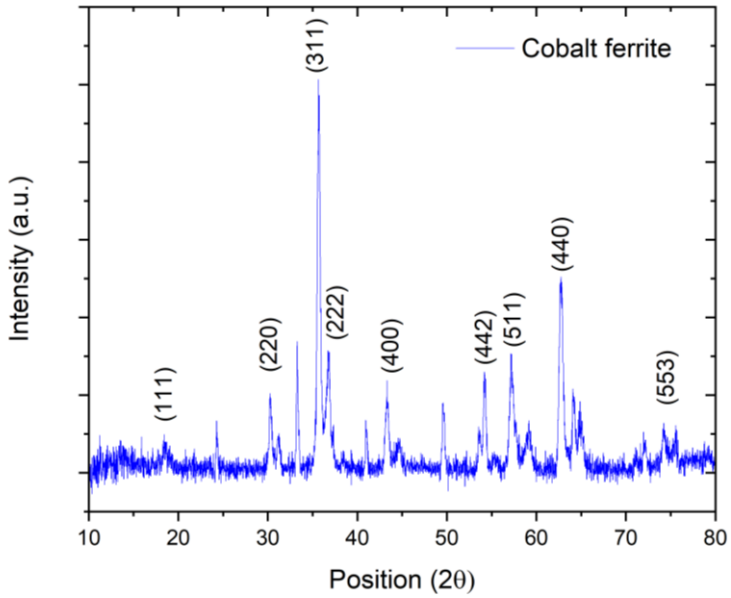

Figure 10. X-ray diffractogram of $CoFe_2O_4$ synthesized.

The most prominent peaks (220), (311) and (440), observed at 2θ values of 30.2°, 35.7°, and 62.6°, are characteristic of the cubic spinel structure of $CoFe_2O_4$. The strongest reflection at 35.7° confirms that cobalt ferrite is the primary phase in the material, as validated by the reference card 96-153-3164 from the Crystallography Open Database (COD). Similar X-ray diffractogram have been reported for $CoFe_2O_4$ particles synthesized via sol-gel [24], co-precipitation [51, 52], and solution combustion synthesis [53].

In addition to the primary cobalt ferrite peaks, smaller peaks are also observed in the diffractogram, which may indicate the presence of hematite (Fe_2O_3). The presence of this secondary phase can be attributed to the partial oxidation of iron during synthesis, leading to the formation of hematite, these peaks at 23.9° and 32.97°, for example, are in agreement with those reported for hematite in cobalt ferrite materials prepared by the sol-

gel method [24, 54]. Despite this, these minor peaks are much less intense compared to those of $CoFe_2O_4$, suggesting that the cobalt ferrite phase is dominant and that the sample exhibits good overall crystallinity.

A comparison between the experimental XRD data and the reference diffraction patterns, shown in Figure 11, further confirms the phase identity. The experimental peaks align well with the reference pattern, reinforcing the conclusion that $CoFe_2O_4$ is the main phase present in the sample.

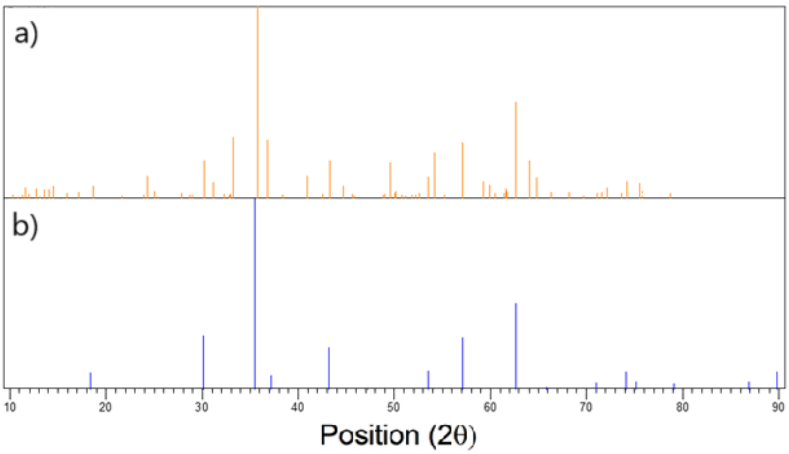

Figure 11. Comparison between the a) experimental XRD data and b) the reference diffraction patterns of the reference card 96-153-3164 that represents $CoFe_2O_4$.

The crystallite sizes of the cobalt ferrite nanoparticle obtained using the Size-Strain Plot (SSP) and Halder-Wagner methods were 20.10 nm and 19.23 nm, respectively. These values are typical of nanomaterials, are in close agreement with each other, and also align well with those obtained in previous work [50]

4.1.2. Fourier Transform Infrared Spectroscopy

Figure 12 shows the FTIR spectra for $CoFe_2O_4$, $CoFe_2O_4$@C and $CoFe_2O_4$@SiO_2, demonstrating distinct transmittance behaviors that reflect the presence of cobalt ferrite and the influence of the carbon and silica coatings.

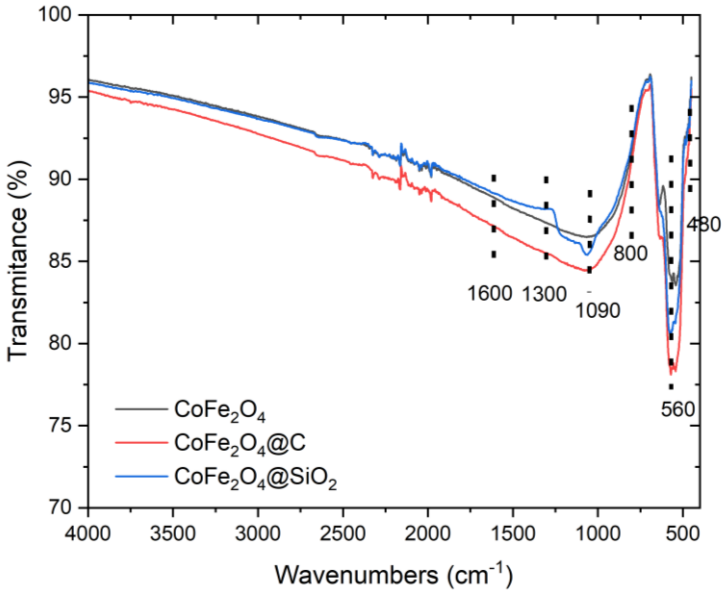

Figure 12. FTIR spectra of the catalysts.

All the samples exhibited strong peaks at 560 cm^{-1} and 480 cm^{-1}, characteristic of the metal-oxygen stretching vibrations (Fe-O and Co-O, respectively) typical of the spinel structure, confirming the composition of the cobalt ferrite [24].

The $CoFe_2O_4$@C spectrum showed consistently lower transmittance at all wavenumbers, especially noticeable in the range of 4000 to 800 cm^{-1}, which may be due to the carbon coating, which introduces various organic functional groups to the metal. Specifically, the peaks between 1600 and 1100 cm^{-1} can be attributed to the C-OH, -OH, C=C and C-H bond stretching interactions [48].

In the $CoFe_2O_4$@SiO_2 spectrum, it is possible to observe a spare peak between 1270 and 990 cm^{-1}, and especially near 1090 cm^{-1}, characteristic of the Si-O-Si stretching and bending modes, confirming the presence of a silica coating on the cobalt ferrite core [24]. The higher overall transmittance of the $CoFe_2O_4$@SiO_2 sample compared to $CoFe_2O_4$@C is consistent with the transparency of silica in the infrared region, except for the specific bands related to Si-O.

These FTIR spectra confirm the composition and coatings of the samples: the cobalt ferrite is identifiable by its Fe-O and Co-O bands, while the carbon and silica coatings contribute with additional vibrational bands unique to each material.

4.1.3. Textural Properties

The nitrogen sorption isotherms of the $CoFe_2O_4$, $CoFe_2O_4$@C and $CoFe_2O_4$@SiO_2 samples are shown in Figure 13.

It can be observed that all the materials exhibit typical Type IVa isotherms with hysteresis loops, which are characteristic of mesoporous materials according to the IUPAC classification [46]. This type of isotherm indicates that adsorption initially occurs as monolayers on the pore walls, followed by multilayer adsorption and, eventually, capillary condensation within the mesopores. The hysteresis loops observed are most likely of the H3 type, which are often associated with non-rigid aggregates of plate-like particles and slit-shaped pores, where the pore network may include larger pores that are not completely filled with condensate.

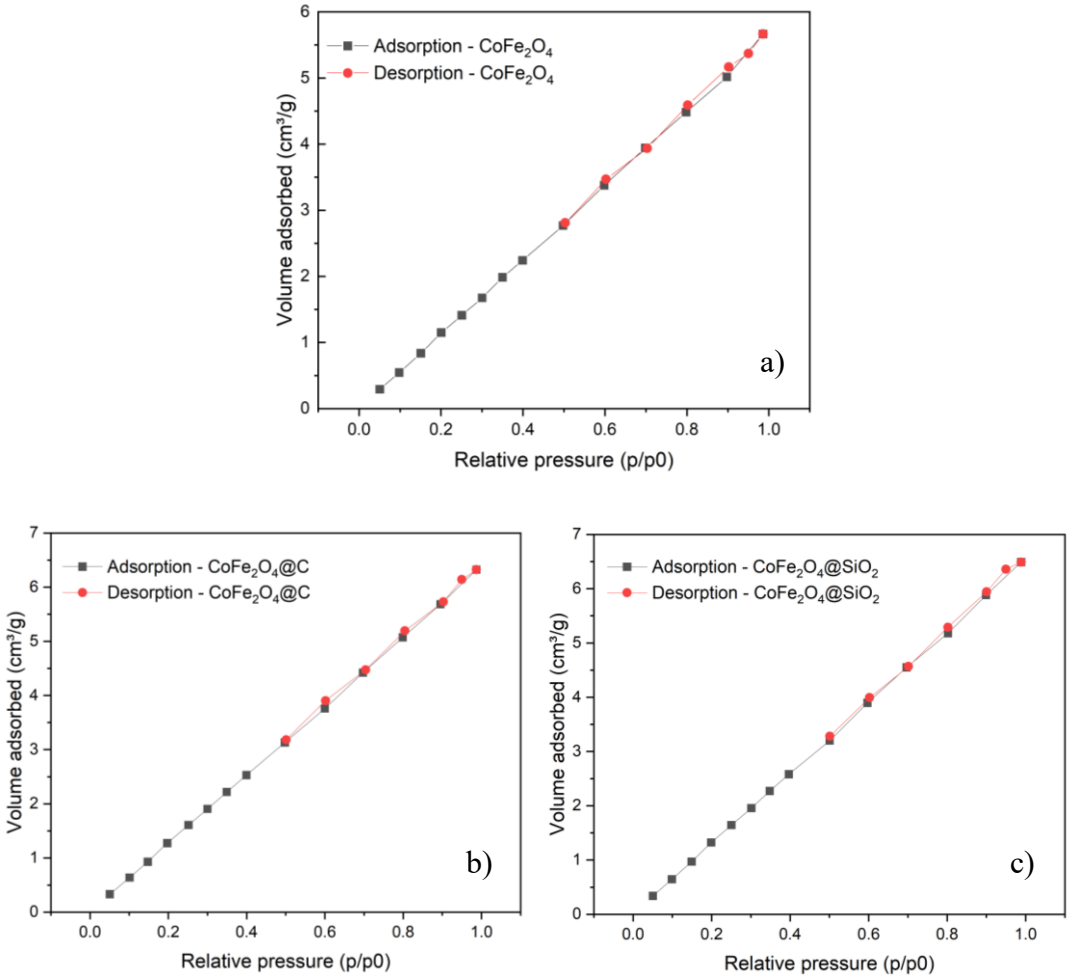

Figure 13. Adsorption isotherms of N_2 at 77 K of a) $CoFe_2O_4$, b) $CoFe_2O_4$@C and c) $CoFe_2O_4$@SiO_2.

The BET surface areas and total pore volumes of the materials were evaluated and are shown in Table 2.

Table 2: Textural properties of the synthesized catalysts.

Material	S_{BET} (m^2/g)	Total pore Volume (mm^3/g)
$CoFe_2O_4$	9	8.786
$CoFe_2O_4$@C	10	9.804
$CoFe_2O_4$@SiO_2	10	10.066

It is possible to observe that the $CoFe_2O_4$ sample exhibited the lowest BET surface area and pore volume, resulting in a less steep adsorption curve in the isotherm and limited adsorption capacity, characteristic of mesoporous materials with fewer active sites. Previous works carried out by the group also reported a surface area of 9 m^2/g for a cobalt ferrite obtained under similar conditions [24]. Coating $CoFe_2O_4$ with carbon ($CoFe_2O_4$@C) slightly increased the surface area to 10 m^2/g and pore volume to 9.804 mm^3/g, consistent with similar findings for carbon-coated materials in the literature [24, 54, 55]. The $CoFe_2O_4$@SiO_2 sample, with a silica coating, also showed a surface area of 10 m^2/g, but a slight increase in pore volume (10.066 mm^3/g), resulting in the most pronounced adsorption isotherm compared to the other two materials, likely due to the formation of accessible mesoporous silica networks, aligning with observations from studies on silica-coated mesoporous nanoparticles [56, 57].

Although coating $CoFe_2O_4$ with carbon or silica resulted in slight increases in surface area and pore volume, the values are very close, and considering potential errors associated with the analysis process, it is not certain that one is significantly greater than the other. Overall, the consistently low BET surface area and pore volume observed across all samples suggest that $CoFe_2O_4$ and its coated forms lack the extensive surface area and accessible pore networks typically required for high-performance adsorption, indicating that they are not highly effective adsorbent materials.

4.1.4. Contact Angle

In Table 3 are presented the approximate contact angles measured between water droplets and various materials, accompanied by images illustrating the droplet formation on each surface.

Table 3. Contact angle for each material.

Material	Contact Angle (°)	Representative Image
$CoFe_2O_4$	130 ± 2	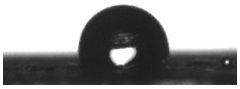
$CoFe_2O_4$@C	65 ± 2	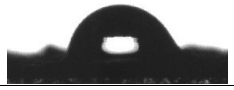
$CoFe_2O_4$@SiO_2	41 ± 2	

According to literature, a material is classified as hydrophobic if its contact angle exceeds 90°, and hydrophilic if the contact angle is below 90° [49]. Additionally, nanoparticulate magnetic materials like cobalt ferrite are often coated with a hydrophilic binder shell to reduce their hydrophobicity [50]. As shown in the table, uncoated cobalt ferrite is hydrophobic with a contact angle of 130°, while its carbon- and silica-coated versions demonstrate increased hydrophilicity, with reduced contact angles of 65 and 41°, respectively. Other works reported values for silica particles in the range of 17-145° depending on the amount of silanol (Si-OH) groups on the silica surface [58]. Carbon materials have reported contact angle values varying in the range 75-127° [59], which is greatly influenced by the surface functional groups. It should also be noted that the surface roughness may heavily influence the measurement of contact angles via sessile drop methodology [60,61]. Similarly, the method of immobilization of the powdered sample may also affect the results [43], rendering it difficult to directly compare the results obtained here.

4.2. Analytic Methods

4.2.1. Quinoline Adsorption

The adsorption of quinoline by the three cobalt ferrite-based materials was studied during the experimental period, as shown in Figure 14.

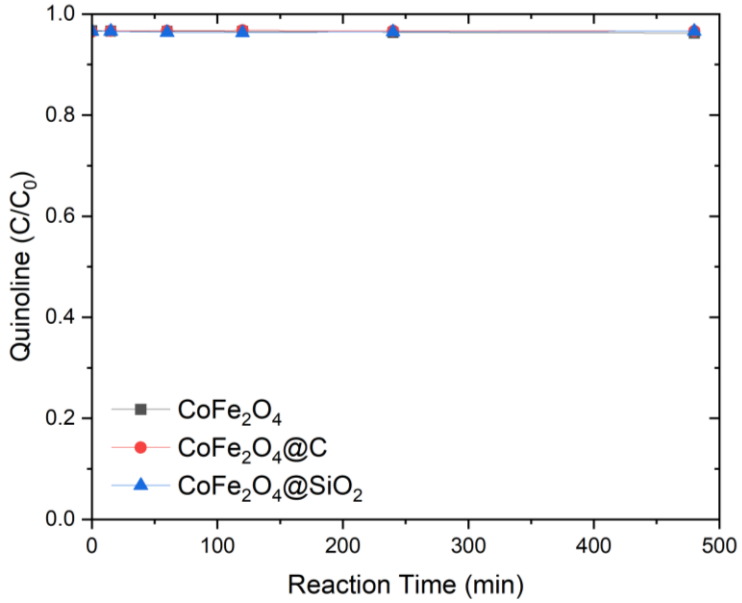

Figure 14. Adsorption of quinoline by each material. The lines are only intended to guide the eyes.

The results showed that all the materials adsorbed an insignificant amount of quinoline. Overall adsorption was minimal, which suggests that cobalt ferrite-based materials are not effective at removing quinoline from solution through adsorption.

In Figure 13, the adsorption isotherms showed low adsorption of gaseous nitrogen, a molecule smaller than quinoline, for all three materials, supporting the possibility that cobalt ferrite-based materials are not highly effective adsorption materials, especially for larger organic molecules such as quinoline.

4.2.2. Oxidative Denitrogenation of Simulated Fuel

4.2.2.1. H_2O_2 Decomposition in Aqueous Phase

The decomposition of H_2O_2 in the biphasic oxidation processes carried out with the $CoFe_2O_4$-based catalysts and in the non-catalytic (N.C.) run was analyzed by UV-VIS spectrophotometry and its behavior is shown in Figure 15.

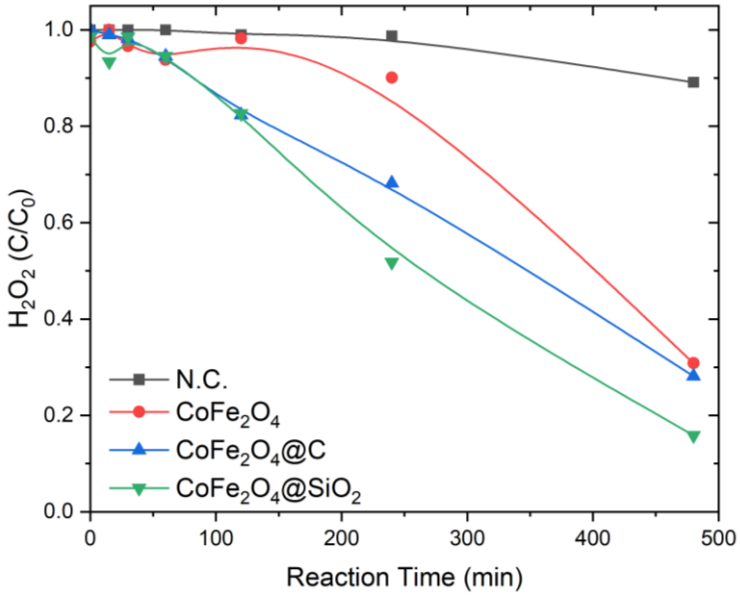

Figure 15. H_2O_2 decomposition during the reaction time. The lines are only intended to guide the eyes.

In the non-catalytic run, around 90% of the initial H_2O_2 remained after 480 minutes of reaction, demonstrating that, in the absence of a catalyst, the natural decomposition of hydrogen peroxide is slow.

The reactions carried out in the presence of the catalysts showed greater decomposition of hydrogen peroxide, with the $CoFe_2O_4$ metal core being the least efficient catalyst compared to its coated versions; the concentration of H_2O_2 decreased steadily during the experiment, with around 30% of the initial H_2O_2 remaining at the end of the experiment. The $CoFe_2O_4$@C catalyst showed moderate efficiency in the decomposition of H_2O_2. As time passed, there was a steady decrease in the concentration of H_2O_2. At the end of the 480-minute reaction, approximately 28% of the initial H_2O_2 remained in the reaction medium.

The $CoFe_2O_4$@SiO_2 catalyst performed better than the other two. At the end of the experiment, around 84% of the initial H_2O_2 had been decomposed in the reaction medium, indicating that the silica coating increases the catalytic activity of the $CoFe_2O_4$ core for the decomposition of H_2O_2. It was also this reaction that decomposed the peroxide most quickly, at minute 240 it had already decomposed just over half of the initial concentration.

The rate of the decomposition of hydrogen peroxide may be linked to the hydrophilicity/hydrophobicity of the samples, previously discussed in section 4.1.4. The coated particles ($CoFe_2O_4$@C and $CoFe_2O_4$@SiO_2) both resulted in contact angles lower

than 90°, being thus mostly located in the aqueous phase. The pure core $CoFe_2O_4$ resulted in a higher contact angle (130°), which means it is preferably located in the organic phase. Given that the hydrogen peroxide is located in the water phase, particles preferably located at the water phase will likely interact better with the reactant. Previous works on the treatment of oily wastewater by oxidation have shown that the more hydrophilic a particle is, the higher is its ability to decompose hydrogen peroxide [63, 64].

4.2.2.2. Concentration of Quinoline in Organic Phase

The presence of quinoline in the organic phase during ODN for each catalyst is shown in Figure 16.

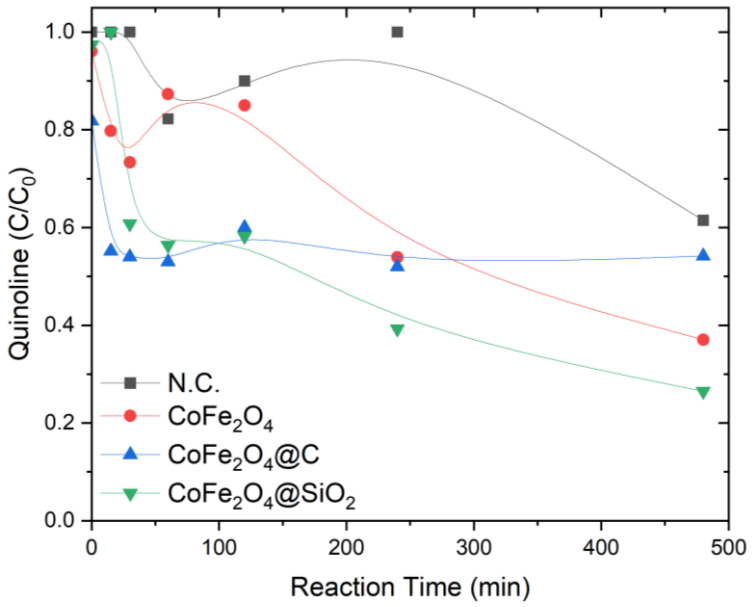

Figure 16. Concentration of quinoline in the organic phase by reaction time. The lines are only intended to guide the eyes.

It can be seen that the non-catalytic reaction has a lower quinoline removal rate than the other experiments, with a slow decrease, with around only 38% of quinoline removed from the organic phase at the end of the process; compared to the catalytic reactions, the contaminant removal efficiency is poor.

On the other hand, the cobalt ferrite metal core ($CoFe_2O_4$) shows a more consistent and gradual decrease over time, but still with a relatively slow removal rate. At the end of the reaction 62% of the initial quinoline is removed. The carbon coating showed a rapid decrease in the amount of quinoline in the organic phase, improving catalytic performance and increasing the removal process, but remained stable until the end of the process, removing around 45% of the quinoline.

The catalyst that proved to be most efficient in removing quinoline was $CoFe_2O_4@SiO_2$, with a strong initial catalytic effect followed by a low concentration of quinoline over the reaction time, leaving only 26% of quinoline in the organic phase.

4.2.2.3. Quinoline in Aqueous Phase

The variation of the quinoline concentration with time in the aqueous phase is presented in Figure 17.

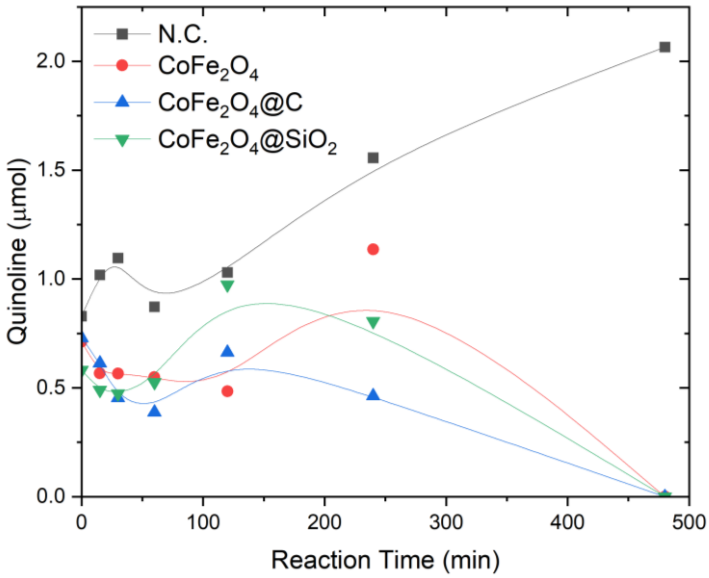

Figure 17. Concentration of quinoline in aqueous phase. The lines are only intended to guide the eyes.

In the non-catalytic reaction, it is possible to observe the gradual accumulation of quinoline, which passes from the organic phase to the aqueous phase, due to mass transfer between the phases, without significant degradation of quinoline until the end of this reaction.

The three catalytic reactions typically showed a peak increase in the amount of quinoline in the aqueous phase followed by a decrease, tending to zero, suggesting that after passing from the organic to the aqueous phase the quinoline was degraded. The uncoated metal core was the catalyst that took the longest to reach this peak, at around 240 minutes of reaction, but then quickly degraded the quinoline.

The catalysts coated with carbon and silica showed similar curves, with peaks at around 120 minutes, earlier than the metallic core, however $CoFe_2O_4@SiO_2$ had a peak with a greater amount of quinoline than the carbon-coated one, so the amount of quinoline

degraded was also greater, since at the end of the reactions the amount of quinoline in the aqueous phase was very small.

The results of section 4.2.2.1 on the decomposition of H_2O_2 help to clarify the behavior of quinoline degradation in the aqueous phase, highlighting the relationship between the catalytic activity and the hydrophilicity of the materials. As hydrogen peroxide is present in the aqueous phase, the more hydrophilic $CoFe_2O_4$@SiO_2 catalyst decomposed the H_2O_2 more efficiently and consequently generated reactive hydroxyl species more efficiently, accelerating the oxidation of quinoline after its transfer from the organic phase. This is reflected in the earlier and more pronounced degradation of quinoline, with the peak concentration occurring earlier than with other catalysts. In contrast, the slower decomposition of H_2O_2 observed with the more hydrophobic and uncoated $CoFe_2O_4$ leads to a delayed peak in quinoline concentration, highlighting how the hydrophilicity of a catalyst influences both the decomposition of the oxidant hydrogen peroxide and the removal of quinoline.

4.2.3. Intermediate Compounds of Quinoline Oxidation

The aqueous and organic phases of the quinoline catalytic oxidation reaction in the biphasic medium were analyzed by gas chromatography-mass spectrometry (GC-MS) to study the different compounds present during the reaction. In Figure 18 is possible to visualize the mass spectra of quinoline.

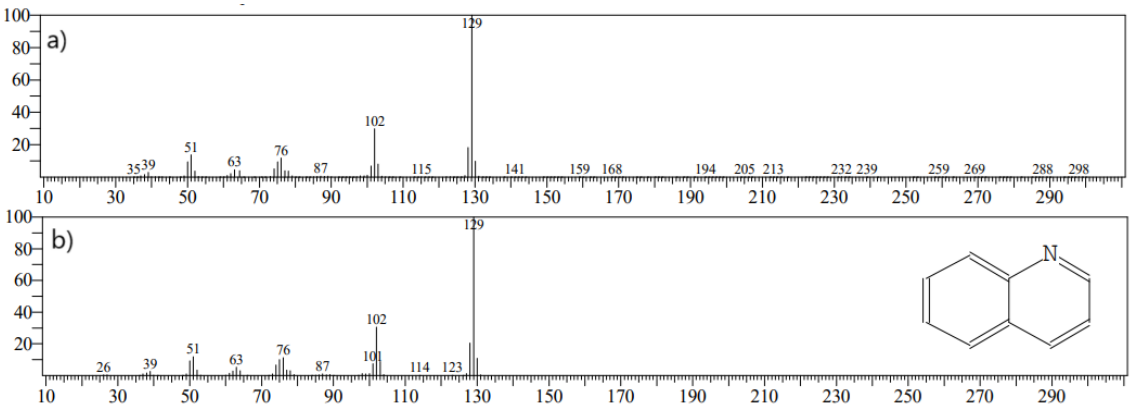

Figure 18. a) Mass spectra found and b) mass spectra of quinoline, that matches a).

Quinoline was identified and its behavior was studied. Initially, its concentration increased, followed by a decrease throughout the reaction. This suggests the transfer of quinoline to the aqueous phase and its subsequent removal, which is consistent with the results of HPLC analyses of the aqueous phase of quinoline in catalytic reactions. In

addition, intermediates resulting from the oxidation of long-chain hydrocarbons in the organic phase were identified, including 1-decanol, pentadecane and heneicosane, which could arise from partial oxidation of the isooctane phase. A previous work carried out in the group identified that isooctane could undergo oxidation under the conditions studied, observing an increase in the total organic compounds in the water phase representing 0.002-0.013 wt.% of the isooctane introduced in the system [65]. Even though the value reported is low and may not affect quinoline oxidation, it may explain the detection of long-chain carbon compounds. The detection of (Z)-9-octadecenamide after 240 minutes suggests the formation of nitrogen-containing intermediates during quinoline oxidation. In Figure 19 is possible to observe the compounds found in the aqueous phase by GC-MS.

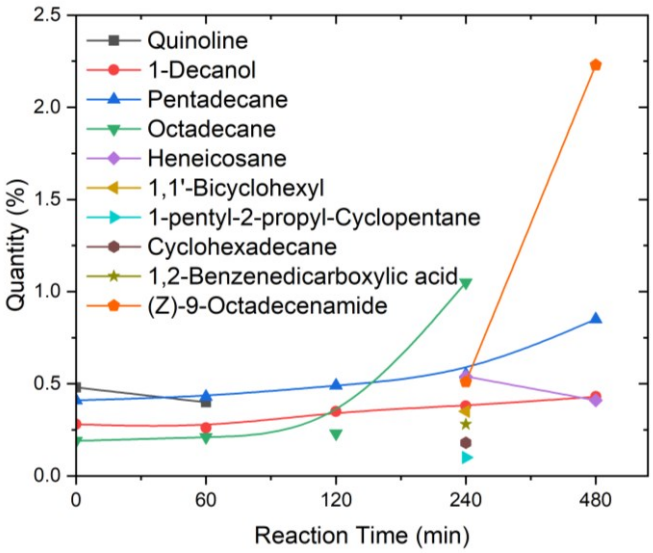

Figure 19. Compounds found in the aqueous phase by GC-MS. The lines are only intended to guide the eyes.

The organic phase, in addition to the presence of quinoline, presented a more diverse set of compounds, some of which are shown in Figure 20.

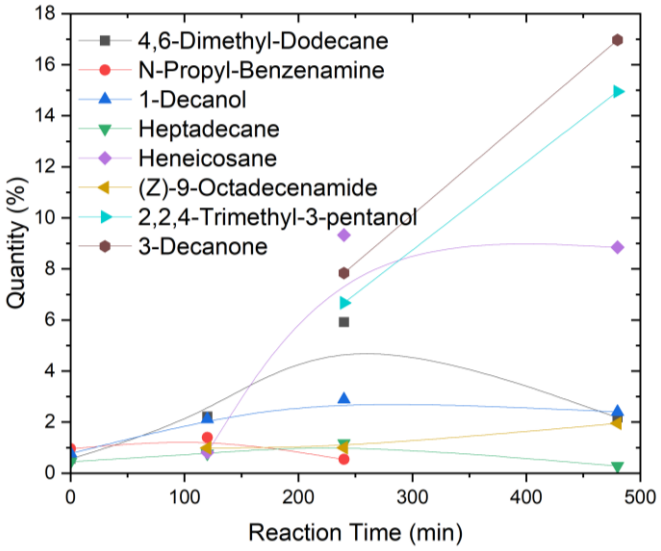

Figure 20. Compounds found in the organic phase by GC-MS. The lines are only intended to guide the eyes.

Initially, quinoline represented almost 80% of the sample analyzed, but at the end of the reaction it represented less than 1%, indicating its gradual degradation. Several nitrogen-containing intermediate products were identified throughout the reaction, as N-propyl-benzenamine that reached its maximum at 120 minutes with a concentration of 1.4% before becoming undetectable, suggesting that the pyridine ring is broken during oxidation. Products arising from the breaking of the pyridine ring during quinoline oxidation have been previously reported [66]. (Z)-9-octadecenamide was present throughout the reaction, increasing to 1.95% at the end. Other nitrogen compounds, such as N-nitro-N-octyl-1-octanamine, N-tert-butoxycarbonylimidazole and N-(1-methyl-2-{4-[(1-methylethyl)sulfanyl]phenyl}-2-[(trimethylsilyl)oxy]ethyl)octan-1-amine, were also detected. Similar to the aqueous phase, 1-decanol, heneicosane and its isomer, among other long-chain hydrocarbons, were present during the reaction, which could be a result of the partial oxidation of isooctane.

Previous works have reported a range of possible intermediates during quinoline oxidation in aqueous phase considering distinct oxidants [67-69], from small chain carboxylic acids to compounds still containing the benzene and pyridinic rings, highlighting the complex route in which quinoline is oxidized. No clear consensus in the literature could be found for the oxidation of quinoline.

4.2.4. Total Organic Carbon

The aqueous phase was also analyzed to observe the total amount of organic carbon during the quinoline oxidation experiments, and its behavior according to each reaction can be seen in Figure 21.

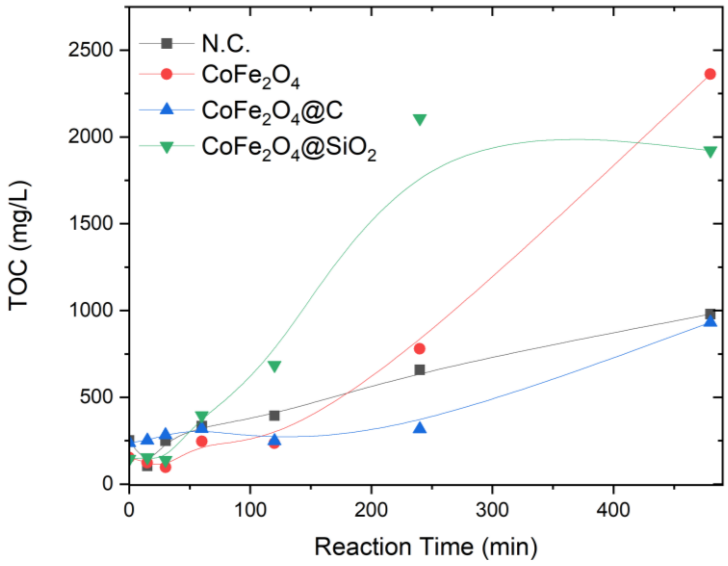

Figure 21. TOC evolution for each reaction run. The lines are only intended to guide the eyes.

The concentration of TOC in the non-catalytic reaction shows a gradual increase in organic content, which may indicate the mass transfer of quinoline from the organic phase to the aqueous phase without significant degradation. This is in line with the HPLC observations made for the non-catalytic reaction. Furthermore, the inorganic carbon (IC) values remained relatively stable, indicating that quinoline remained unaltered in the aqueous phase, with minimal conversion to inorganic carbon or other by-products. This finding aligns with the hypothesis that the target compound did not suffer significant degradation during this reaction.

In contrast, the catalytic reactions are initially characterized by a peak in TOC at approximately 120 minutes for the $CoFe_2O_4$@C and $CoFe_2O_4$@SiO_2 catalysts, indicating that these catalysts effectively facilitate the transfer of quinoline to the aqueous phase. As observed in HPLC, after reaching a peak, the concentration of quinoline tends to decrease to zero, which increases the amount of inorganic carbon and decreases the total organic carbon, this suggests that quinoline is being mineralized.

4.2.5. Oxidative Denitrogenation Using $CoFe_2O_4$ as Catalyst

Oxidative nitrogen removal using specific cobalt ferrite catalysts has not yet been extensively studied, but it is possible to compare the quinoline conversion results of this work with two previously cited references Ogunlaja *et al*. (2019) [14] and Banisharif *et al.* (2019) [37], in Section 2.6, related to ODN, as shown in Table 4.

Table 4. Comparison between this work and [14,37].

Ref.	Organic Phase	Catalyst	Oxidizer	Extractant	Reaction conditions	Results
[14]	Ethanol with quinoline	Vanadium Oxide (V_2O_5) Supported on Silica (SiO_2)	Terc-Butyl-Hydroperoxide (t-BuOOH)	2,6-Pyridine-Polybenzimidazole (2,6-PyPBI) nanofibers	70° C, 12h, 2.84 g/L	78% total conversion of QN after 12h
[37]	Isooctane with quinoline and toluene	V vanadium-substituted Dawson-type phosphotungstat and heteropolyacid, $H_{11}P_2W_{13}V_5O_{129}$	Hydrogen Peroxide (H_2O_2)	Acetonitrile (C_2H_3N)	70 °C, 7.5 g/L Catalyst	100% QN removal after 30 min
This Work	Isooctane with quinoline	$CoFe_2O_4$ and its coated versions	Hydrogen Peroxide (H_2O_2)	Hydrogen Peroxide (H_2O_2)	80°C, 8h, 1 g/L catalyst	74% QN conversion after 8h

There are several important differences in terms of parameters employed in each work. However, in terms of cost and use of less polluting compounds, it is possible to see some highlights in the method used in this work.

In terms of oxidants, Ogunlaja *et al*. (2019) [14] used tit-butyl hydroperoxide (t-BuOOH), which is a more selective but generally more expensive oxidant, in combination with Vanadium Pentoxide Supported on Silica (V_2O_5/SiO_2) as catalyst, while Banisharif *et al.* (2019) [37] uses H_2O_2 in combination with a vanadium-substituted Dawson-type heteropolyacid catalyst, which clearly allows faster oxidation of quinoline. However, the elaborated reagents required for the synthesis of these catalysts, ammonium metavanadate and vanadium, tungsten and quaternary ammonium silica, respectively, make their synthesis more complex and costly than that of cobalt ferrite.

The extractants used are also quite different. While in this work H_2O_2 acts as both oxidant and extractant, decomposing into O_2 and H_2O, the other two studies use

extractants that are potentially hazardous to the environment, Ogunlaja *et al*. (2019) [14] using nanofibers of 2,6-pyridine-polybenzimidazole (2,6-PyPBI), which are polymeric solid phase adsorbents instead of liquid extractors, and Banisharif *et al.* (2019) [37] using acetonitrile, a traditional liquid phase extractor, which is efficient but expensive and potentially hazardous to the environment due to its toxicity.

In terms of conversion, this work achieved 74% conversion of quinoline in 8h using a concentration of 1g/L of cobalt ferrite, while it took 12h for the catalytic oxidation of quinoline using V_2O_5/SiO_2 to achieve 78% conversion by Ogunlaja *et al*. (2019) [14]. Although the total conversion of quinoline is achieved very quickly, Banisharif *et al*. (2019) [37] used a catalyst concentration of 7.5g/L, which involved vanadium and tungsten in its preparation, leading to considerably higher production costs for this high concentration.

Thus, in terms of cost and ecology, this work is less expensive and more environmentally friendly compared to other catalytic systems.

CONCLUSIONS AND FUTURE WORK

5. CONCLUSIONS

This study aimed to synthesize metallic nanoparticles coated with silica and carbon for application in denitrogenation processes. The characterization has confirmed the successful formation of the cobalt ferrite structure and the integrity of the coatings. Notably, the carbon and silica coatings significantly altered the properties of the metallic core, especially regarding hydrophobicity. Contact angle measurements showed a transition from the hydrophobic nature of $CoFe_2O_4$ to a more hydrophilic surface due to the coatings.

In terms of catalytic performance, $CoFe_2O_4@SiO_2$ was the most effective catalyst for both H_2O_2 decomposition and quinoline removal, outperforming the other catalysts due to its hydrophilic surface. This enhanced hydrophilicity not only improved H_2O_2 decomposition but also facilitated more efficient quinoline removal, as it promoted a greater generation of reactive oxygen species essential for the quinoline oxidation process. Additionally, the uncoated cobalt ferrite exhibited less favorable results, likely due to its higher susceptibility to leaching in the absence of coatings.

The degradation pathways of quinoline were thoroughly explored, with GC-MS analysis identifying several intermediates, demonstrating the complexity of the reaction mechanisms. TOC analysis confirmed that catalytic processes result in significant quinoline degradation, while non-catalytic reactions mainly drive mass transfer without substantial degradation.

In conclusion, this work underscores the potential of cobalt ferrite-based catalysts for environmental applications, particularly in treating nitrogen-containing organic pollutants. The findings suggest a promising approach for developing cost-effective and environmentally friendly catalytic systems for treating nitrogen-containing organic pollutants, thereby contributing to the advancement of sustainable chemical processes.

6. FUTURE WORK

Future work should focus the optimization of the process to improve catalytic performance and quinoline removal efficiency by adjusting the operating parameters, such as the ratio between the aqueous and organic phases, the reaction temperature, the concentration of hydrogen peroxide and catalyst, as well as recovery studies. Other types of metal catalyst synthesis and their performance in quinoline removal should also be tested.

It is also important to analyze $CoFe_2O_4$ by transmission electron microscopy (TEM), scanning electron microscopy (SEM) and thermogravimetric analysis (TGA) to correlate structural and morphological characteristics with catalytic performance, facilitating the design of more effective catalysts for denitrogenation processes. Studying the application of these metal catalysts to other compounds present in fossil fuels is also a necessary step.

In addition, a more in-depth analysis of the properties of the catalysts after the reactions will provide valuable information on their stability, possible deactivation and structural changes. This will help to refine their use in repetitive cycles and long-term applications.

REFERENCES

7. REFERENCES

[1] X. Hao, H. An, H. Qi, and X. Gao, "Evolution of the exergy flow network embodied in the global fossil energy trade: Based on complex network," *Applied Energy*, vol. 162, pp. 1515-1522, 2016. doi: 10.1016/j.apenergy.2015.04.032.

[2] E. Institute, *Statistical review of world energy*, Jun. 2023. [Online]. Available: https: //www.energyinst.org/statistical-review.

[3] I. E. Agency, *World energy outlook,* 2023. [Online]. Available: https://www.iea. org/reports/world-energy-outlook-2023.

[4] Z. Zaidi, Y. Gupta, S. L. Gayatri, and A. Singh, "A comprehensive discussion on fuel combustion and desulfurization technologies," *Inorganic Chemistry Communications*, vol. 154, p. 110 964, 2023. doi: 10. 1016/j.inoche.2023.110964.

[5] G. H. C. Prado, Y. Rao, and A. de Klerk, "Nitrogen removal from oil: A review," *Energy & Fuels*, vol. 31, no. 1, pp. 14-36, 2017. doi: 10.1021/ acs.energyfuels.6b02779.

[6] H. Yang, J. Chen, C. Fairbridge, Y. Briker, Y. J. Zhu, and Z. Ring, "Inhibition of nitrogen compounds on the hydrodesulfurization of substituted dibenzothiophenes in light cycle oil," *Fuel Processing Technology*, vol. 85, no. 12, pp. 1415-1429, 2004. doi: 10.1016/j.fuproc.2003.09.008.

[7] European Commission. "*Regulation (EU) No 582/2011 of the Commission of 25 May 2011*." (2011), [Online]. Available: http://data.europa.eu/eli/reg/2011/582/oj.

[8] European Commission. "*Commission proposes new Euro 7 standards to reduce vehicle emissions and improve air quality*." (2022), [Online]. Available: https://ec.europa.eu/commission/presscorner/detail/pt/ip_22_6495.

[9] S. S. Bello, C. Wang, M. Zhang, *et al.,* "A review on the reaction mechanism of hydrodesulfurization and hydrodenitrogenation in heavy oil upgrading," *Energy & Fuels*, vol. 35, no. 14, pp. 10 998-11 016, 2021. doi: 10.1021/ acs.energyfuels.1c01015.

[10] M. M. H. Mondol, I. Ahmed, H. J. Lee, A. Morsali, and S. H. Jhung, "Metal-organic frameworks and metal-organic framework-derived materials for denitrogenation of liquid fuel via adsorption and catalysis," *Coordination Chemistry Reviews*, vol. 495, p. 215 382, 2023. doi: 10.1016/j.ccr.2023. 215382.

[11] S. Mirshamsi, Y. Yan, S. Kamal, *et al.,* "Thermal behavior of nitrogen oxides relevant to oxidative denitrogenation," *The Journal of Chemical Thermodynamics*, vol. 136, pp. 28-43, 2019. doi: 10.1016/j. jct.2019.04.014.

[12] F. F. Roman, J. L. Diaz de Tuesta, A. M. T. Silva, J. L. Faria, and H. T. Gomes, "Carbon-based materials for oxidative desulfurization and denitrogenation of fuels: A review," *Catalysts,* vol. 11, no. 10, p. 1239, 2021. doi: 10.3390/catal11101239.

[13] S. H. Ammar, Y. S. Kareem, and M. S. Mohammed, "Catalytic-oxidative/adsorptive denitrogenation of model hydrocarbon fuels under ultrasonic field using magnetic reduced graphene oxide-based phosphomolybdic acid (PMo-Fe_3O_4/rGO)," *Ultrasonics Sonochemistry*, vol. 64, p. 105 050, 2020. doi: 10.1016/j.ultsonch.2020.105050.

[14] A. Ogunlaja, M. Abdul-quadir, P. Kleyi, *et al.*, "Towards oxidative denitrogenation of fuel oils: Vanadium oxide-catalyzed oxidation of quinoline and adsorptive removal of quinoline-n-oxide using 2,6-pyridine-polybenzimidazole nanofibers," *Arabian Journal of Chemistry,* vol. 12, no. 2, pp. 198-214, 2019. doi: 10.1016/j.arabjc.2017.05.010.

[15] I. Ahmed and S. H. Jhung, "Adsorptive desulfurization and denitrogenation using metal-organic frameworks," *Journal of Hazardous Materials*, vol. 301, pp. 259-276, 2016. doi: 10.1016/j.jhazmat.2015.08.045.

[16] A. Haruna, Z. M. A. Merican, and S. G. Musa, "Recent advances in catalytic oxidative desulfurization of fuel oil - a review," *Journal of Industrial and Engineering Chemistry*, vol. 112, pp. 20-36, 2022. doi: 10.1016/j.jiec.2022.05.023.

[17] S. Vedachalam and A. K. Dalai, "Hydrotreating and oxidative desulfurization of heavy fuel oil into low sulfur marine fuel over dual function NiMo/–Al_2O_3 catalyst," *Catalysis Today,* vol. 407, pp. 165-171. doi: 10.1016/j.cattod.2022.01.013.

[18] Y. Liu, C. Deng, P. Wu, *et al.,* "High-entropy zeolitic imidazolate framework for efficient oxidative desulfurization of diesel fuel: Towards complete sulfur removal and valuable sulfone production," *Fuel,* vol. 359, p. 130 375, 2024. doi: 10.1016/j.fuel.2023.130375.

[19] J. F. Palomeque-Santiago, R. López-Medina, R. Oviedo-Roa, *et al.*, "Deep oxidative desulfurization with simultaneous oxidative denitrogenation of diesel fuel and straight

run gas oil," *Applied Catalysis B: Environmental,* vol. 236, pp. 326-337, 2018. doi: 10.1016/j.apcatb.2018.04.079.

[20] M. Jafarian, B. B. Dally, and G. J. Nathan, "Hydrogen peroxide for fuel oxidation to achieve CO_2 capture from lime production," *Energy Conversion and Management: X*, vol. 15, p. 100 276, 2022. doi: 10.1016/j.ecmx.2022.100276.

[21] R. V. Mambrini, C. Z. Maia, J. D. Ardisson, P. P. de Souza, and F. C. C. Moura, "Fe/C and FeMo/C hybrid materials for the biphasic oxidation of fuel contaminants," *New Journal of Chemistry.,* vol. 41, pp. 142-150, 2017. doi: 10.1039/C6NJ02718K.

[22] I. R. Guimarães, A. S. Giroto, W. F. de Souza, and M. C. Guerreiro, "Highly reactive magnetite covered with islands of carbon: Oxidation of N and S-containing compounds in a biphasic system," *Applied Catalysis A: General,* vol. 450, pp. 106- 113, 2013. doi: 10.1016/j.apcata.2012.10.017.

[23] W.-j. Liu, Y.-x. Liu, X.-y. Yan, G.-p. Yong, Y.-p. Xu, and S.-m. Liu, "One-pot synthesis of yolk-shell mesoporous carbon spheres with high magnetization," *Journal of Materials Chemistry A*, vol. 2, pp. 9600-9606, 2014. doi: 10.1039/C4TA01088D.

[24] A. Silva, F. Roman, A. Dias, *et al.*, "Hybrid multi-core shell magnetic nanoparticles for wet peroxide oxidation of paracetamol: Application in synthetic and real matrices," *Journal of Environmental Chemical Engineering*, vol. 11, 2023. doi: 10.1016/j.jece.2023.110806.

[25] A. Gupta, Anjali, and M. Sahni, "Structural and magnetic properties of cobalt ferrite nano-particles," *Materials Today: Proceedings,* 2023. doi: 10.1016/j.matpr.2023.09.121.

[26] M. Houshiar, F. Zebhi, Z. J. Razi, A. Alidoust, and Z. Askari, "Synthesis of cobalt ferrite ($CoFe_2O_4$), nanoparticles using combustion, coprecipitation, and precipitation methods: A comparison study of size, structural, and magnetic properties," *Journal of Magnetism and Magnetic Materials*, vol. 371, pp. 43-48, 2014. doi: 10.1016/j.jmmm.2014.06.059.

[27] N. Rey-Raap, S. F. Villanueva, J. A. Menéndez, and A. Arenillas, "Microporous carbon spheres derived from resorcinol-formaldehyde solutions. a new approach to coat supports," *Microporous and Mesoporous Materials*, vol. 252, pp. 154-160, 2017. doi: 10.1016/j.micromeso.2017.06.018.

[28] A. M. Demin, A. V. Vakhrushev, M. S. Valova, *et al.*, "Features of doxorubicin adsorption on Fe O magnetic nanoparticles coated with SiO_2 or SiO_2/aminopropylsilane," *Mendeleev Communications*, vol. 33, no. 2, pp. 160-163, 2023. doi: 10.1016/j.mencom.2023.02.004.

[29] A. B. Lozada, A. Sango, A. Sangurima-Cedillo, *et al.*, "Mesoporous titanosilicatesilica-coated cobalt ferrite core-shell catalysts for the oxidation of styrene," *Catalysis Today,* vol. 430, p. 114 513, 2024. doi: 10.1016/j.cattod.2024.114513.

[30] N.M.C Guari., A.S. Silva , J-L D. de Tuesta, W.E. Pottker, P.Y Cordeiro, and H.T. Gomes, "Magnetic $CoFe_2O_4$@carbon yolk-shell nanoparticles as catalysts for the catalytic wet peroxide oxidation of paracetamol: Kinetic insights," *Global NEST Journal*, vol. 25, no. 2, pp. 57-66, 2022. doi: 10.30955/gnj.004309.

[31] M. Vafaeezadeh and W. R. Thiel, "Janus interphase catalysts for interfacial organic reactions," *Journal of Molecular Liquids*, vol. 315, p. 113 735, 2020. doi: 10.1016/j.molliq.2020.113735.

[32] R. Fang, C. Saggese, S. W. Wagnon, *et al.*, "Effect of nitric oxide and exhaust gases on gasoline surrogate autoignition: Isooctane experiments and modeling," *Combustion and Flame,* vol. 236, p. 111 807, 2022. doi: 10.1016/j.combustflame.2021.111807.

[33] S. Wang, L. Zhou, M. Zheng, J. Han, R. Liu, and J. Yun, "Catalytic ozonation over $Ca_2Fe_2O_5$ for the degradation of quinoline in an aqueous solution," *Industrial & Engineering Chemistry Research,* vol. 61, no. 19, pp. 6343-6353, 2022. doi: 10.1021/acs.iecr.2c00464.

[34] I. Ahmed and S. H. Jhung, "Effective aerobic oxidative denitrogenation of model fuel with metal-free porous carbon derived from phytic acid-loaded polyaniline," *Chemical Engineering Journal*, vol. 479, p. 147 679, 2024. doi: 10.1016/j.cej.2023.147679.

[35] F. Banisharif, M. Dehghani, M. Capel-Sanchez, and J. Campos-Martin, "Extractiveoxidative removals of dibenzothiophene and quinoline using vanadium substituted dawson emulsion catalyst and ionic liquid based solvents," *Journal of Industrial and Engineering Chemistry,* vol. 47, pp. 348-359, 2017. doi: 10.1016/j.jiec.2016.12.005.

[36] A. S. Ogunlaja and O. S. Alade, "Catalyzed oxidation of quinoline in model fuel and the selective extraction of quinoline-n-oxide with imidazoline-based ionic liquids," *Egyptian Journal of Petroleum*, vol. 27, no. 2, pp. 159-168, 2018. doi: 10.1016/j.ejpe.2017.02.004.

[37] F. Banisharif, M. Dehghani, M. Capel-Sanchez, and J. Campos-Martin, "Highly catalytic oxidative desulfurization and denitrogenation of diesel using anchored-silica gel vanadium-substituted dawson-type polyoxometalate," *Catalysis Today,* vol. 333, pp. 219-225, 2019. doi: 10.1016/j.cattod.2018.07.009.

[38] D. F. Silva, R. G. Faria, I. Santos-Vieira, L. Cunha-Silva, C. M. Granadeiro, and S. S. Balula, "Simultaneous sulfur and nitrogen removal from fuel combining activated porous mil-100(Fe) catalyst and sustainable solvents," *Catalysis Today,* vol. 423, p. 114 250, 2023. doi: 10.1016/j.cattod.2023.114250.

[39] X. Jin, X. Du, G. Liu, *et al.*, "Efficient destruction of basic organo-nitrogenous compounds in liquid hydrocarbon fuel using ascorbic acid/ H_2O_2 system under ambient condition," *Journal of Hazardous Materials*, vol. 459, p. 132 242, 2023. doi: 10.1016/j.jhazmat.2023.132242.

[40] Y. Guo, M. Wen, G. Li, and T. An, "Recent advances in voc elimination by catalytic oxidation technology onto various nanoparticles catalysts: A critical review," *Applied Catalysis B: Environmental,* vol. 281, p. 119 447, 2021. doi: 10.1016/j.apcatb.2020.119447.

[41] Y. Guo, Y. Gao, X. Li, *et al.*, "Catalytic benzene oxidation by biogenic pd nanoparticles over 3d-ordered mesoporous CeO_2," *Chemical Engineering Journal*, vol. 362, pp. 41-52, 2019. doi: 10.1016/j.cej.2019.01.012.

[43] E. Nowak, G. Combes, E. H. Stitt, *et al.*, "A comparison of contact angle measurement techniques applied to highly porous catalyst supports," *Powder Technology*, vol. 233, pp. 52-64, January 2013. doi: 10.1016/j.powtec.2012.08.032.

[44] A. S. Silva, M. S. Kalmakhanova, B. K. Massalimova, *et al.*, "Wet peroxide oxidation of paracetamol using acid activated and Fe/Co-pillared clay catalysts prepared from natural clays," *Catalysts*, vol. 9, p. 705, 2019. doi: 10.3390/catal9090705

[45] M. Karimi, J. L. D. de Tuesta, C. N. d. P. Gonçalves, *et al.*, "Compost from municipal solid wastes as a source of biochar for CO_2 capture," *Chemical Engineering & Technology*, vol. 43, no. 7, pp. 1336-1349, 2020. doi: 10.1002/ceat.201900108.

[46] M. Thommes, K. Kaneko, A. V. Neimark, *et al.*, "Physisorption of gases, with special reference to the evaluation of surface area and pore size distribution (IUPAC Technical Report)," *Pure and Applied Chemistry*, vol. 87, no. 9-10, pp. 1051-1069, 2015. doi: 10.1515/pac-2014-1117.

[47] J. Murta, A. P. Ferreira da Silva, C. E. Dos Santos, *et al.*, "The effect of adding alumina as an aluminum source to the diatomaceous earth-based geopolymer," *Engineering Proceedings*, vol. 56, p. 328, 2023. doi: 10.3390/ASEC2023-15907.

[48] M. Lu, Q. Wu, X.-H. Guan, *et al.*, "Preparation of C/$CoFe_2O_4$ nanocomposites based on membrane dispersion-hydrothermal carbonization and their application for dyeing removal," *Desalination and Water Treatment*, vol. 148, pp. 285-295, 2019. doi: 10.5004/dwt.2019.23784.

[49] C. G. Jothi Prakash, R. Prasanth, *et al.*, "Approaches to design a surface with tunable wettability: A review on surface properties," *Journal of Materials Science*, vol. 56, pp. 108-135, 2021. doi: 10.1007/s10853-020-05116-1.

[50] P. H. Nam, L. T. Lu, P. H. Linh, *et al.*, "Polymer-coated cobalt ferrite nanoparticles: Synthesis, characterization, and toxicity for hyperthermia applications," *New Journal of Chemistry*, vol. 42, pp. 14530-14541, 2018. doi: 10.1039/C8NJ01701H.

[51] M. Basak, M. L. Rahman, M. F. Ahmed, *et al.*, "The use of X-ray diffraction peak profile analysis to determine the structural parameters of cobalt ferrite nanoparticles using Debye-Scherrer, Williamson-Hall, Halder-Wagner and Size-strain plot: Different precipitating agent approach," *Journal of Alloys and Compounds*, vol. 895, 2022. doi: 10.1016/j.jallcom.2021.162694.

[52] M. N. Rashin and J. Hemalatha, "Magnetic and ultrasonic studies on stable cobalt ferrite magnetic nanofluid," *Ultrasonic*s, vol. 54, pp. 834-840, 2014. doi: 10.1016/j.ultras.2013.10.009.

[53] B. Jeevanantham, Y. Song, H. Choe, *et al.*, "Structural and optical characteristics of cobalt ferrite nanoparticles," *Materials Letters: X*, vol. 12, December 2021. doi: 10.1016/j.mlblux.2021.100105.

[54] S. Moretto, A. dos S. Silva, J. L. D. de Tuesta, *et al.*, "Comprehensive characterization and development of multi-core shell superparamagnetic nanoparticles for controlled delivery of drugs and their kinetic release modelling," *Materials Today Chemistry,* vol. 33, p. 101748, 2023. doi: 10.1016/j.mtchem.2023.101748.

[55] R. O. Rodrigues, G. Baldi, S. Doumett, *et al.*, "A tailor-made protocol to synthesize yolk-shell graphene-based magnetic nanoparticles for nanomedicine," *Journal of Carbon Research*, vol. 4, no. 4, p. 55, 2018. doi: 10.3390/c4040055.

[56] A. M. Demin, A. I. Maksimovskikh, A. V. Mekhaev, *et al.*, "Silica coating of Fe_3O_4 magnetic nanoparticles with PMIDA assistance to increase the surface area and enhance peptide immobilization efficiency," *Ceramics International*, vol. 47, no. 16, pp. 23078-23087, 15 August 2021. doi: 10.1016/j.ceramint.2021.04.310.

[57] M. Talaei, S. A. Hassanzadeh-Tabrizi, A. Saffar-Teluri, *et al.*, "Synthesis of mesoporous $CuFe_2O_4$@SiO_2 core-shell nanocomposite for simultaneous drug release and hyperthermia applications," *Ceramics International*, vol. 47, no. 21, pp. 30287-30297, 2021. doi: 10.1016/j.ceramint.2021.07.209.

[58] C. Chen, N. Zhang, W. Li, *et al.*, "Water contact angle dependence with hydroxyl functional groups on silica surfaces under CO_2 sequestration conditions," *Environmental Science & Technology*, vol. 49, no. 24, pp. 14680–14687, 2015. doi: 10.1021/acs.est.5b03646.

[59] F. Taherian, V. Marcon, N. F. A. van der Vegt, *et al.*, "What is the contact angle of water on graphene?" *Langmuir,* vol. 29, no. 5, pp. 1457–1465, 2013. doi: 10.1021/la304645w.

[60] Y. Xiao, J. Zheng, Y. He, *et al.*, "Droplet and bubble wetting behaviors: The roles of surface wettability and roughness," *Colloids and Surfaces A: Physicochemical and Engineering Aspects*, vol. 653, p. 130008, 2022. doi: 10.1016/j.colsurfa.2022.130008.

[61] X. Li, D. Banham, F. Feng, *et al.*, "Wettability of colloid-imprinted carbons by contact angle kinetics and water vapor sorption measurements," *Carbon*, vol. 87, pp. 44-60, 2015. doi: 10.1016/j.carbon.2015.01.041.

[62] R. V. Mambrini, A. L. M. Saldanha, J. D. Ardisson, *et al.*, "Adsorption of sulfur and nitrogen compounds on hydrophobic bentonite," *Applied Clay Scienc*e, vol. 83–84, pp. 286-293, 2013. doi: 10.1016/j.clay.2013.08.030.

[63] J. L. Díaz de Tuesta, B. F. Machado, P. Serp, *et al.*, "Janus amphiphilic carbon nanotubes as Pickering interfacial catalysts for the treatment of oily wastewater by selective oxidation with hydrogen peroxide," *Catalysis Today*, vol. 356, pp. 205-215, 2020. doi: 10.1016/j.cattod.2019.07.012.

[64] F. F. Roman, J. L. Díaz de Tuesta, F. K. K. Sanches, *et al.*, "Selective denitrification of simulated oily wastewater by oxidation using Janus-structured carbon nanotubes," *Catalysis Today*, vol. 420, p. 114001, 2023. doi: 10.1016/j.cattod.2023.01.008.

[65] Piccinin, L. (2022). *Catalytic application of carbon nanotubes obtained from plastic solid waste in the removal of quinoline from isooctane by selective oxidation with hydrogen peroxide* (Dissertation). Master's in Chemical Engineering in Instituto Politécnico de Bragança.

[66] Z. Jiao, X. Zhang, H. Gong, *et al.*, "CuO-doped Ce for catalytic wet peroxide oxidation degradation of quinoline wastewater under wide pH conditions," *Journal of Industrial and Engineering Chemistry*, vol. 105, pp. 49-57, 25 2022. doi: 10.1016/j.jiec.2021.10.006.

[67] A. B. Thomsen, H. H. Kilen, *et al.*, "Wet oxidation of quinoline: intermediates and by-product toxicity," *Water Research*, vol. 32, no. 11, pp. 3353-3361, 1998. doi: 10.1016/S0043-1354(98)00116-X.

[68] I. R. Guimarães, L. C. A. Oliveira, P. F. Queiroz, *et al.*, "Modified goethites as catalyst for oxidation of quinoline: Evidence of heterogeneous Fenton process," *Applied Catalysis A: General*, vol. 347, no. 1, pp. 89-93, 2008. doi: 10.1016/j.apcata.2008.06.001.

[69] N. J. Pachupate, P. D. Vaidya, *et al.*, "Catalytic wet oxidation of quinoline over Ru/C catalyst," *Journal of Environmental Chemical Engineering*, vol. 6, no. 1, pp. 883-889, 2018. doi: 10.1016/j.jece.2017.12.014.